

# Reduced-Rank Tensor-on-Tensor Regression and Tensor-variate Analysis of Variance

Carlos Llosa-Vite and Ranjan Maitra

## Abstract

Fitting regression models with many multivariate responses and covariates can be challenging, but such responses and covariates sometimes have tensor-variate structure. We extend the classical multivariate regression model to exploit such structure in two ways: first, we impose four types of low-rank tensor formats on the regression coefficients. Second, we model the errors using the tensor-variate normal distribution that imposes a Kronecker separable format on the covariance matrix. We obtain maximum likelihood estimators via block-relaxation algorithms and derive their asymptotic distributions. Our regression framework enables us to formulate tensor-variate analysis of variance (TANOVA) methodology. Application of our methodology in a one-way TANOVA layout enables us to identify cerebral regions significantly associated with the interaction of suicide attempters or non-attemptor ideators and positive-, negative- or death-connoting words. A separate application performs three-way TANOVA on the Labeled Faces in the Wild image database to distinguish facial characteristics related to ethnic origin, age group and gender.

## Index Terms

CP decomposition, HOLQ, HOSVD, Kronecker separable models, LFW dataset, Multilinear statistics, Multiway regression, Random tensors, Suicide ideation, Tensor Train format, Tensor Ring format, Tucker format

## I. INTRODUCTION

The classical simple linear regression model (without intercept) relates the response variable  $y_i$  to the explanatory variable  $x_i$  for  $i = 1, 2, \dots, n$  as

$$y_i = \beta x_i + e_i, \quad \text{Var}(e_i) = \sigma^2,$$

where  $\beta$  is the regression coefficient parameter and  $\sigma^2$  is the variance parameter of the errors. A natural extension of simple linear regression for vector-valued response and explanatory variables is the multivariate linear regression model

$$\mathbf{y}_i = B\mathbf{x}_i + \mathbf{e}_i, \quad \text{Var}(\mathbf{e}_i) = \Sigma, \quad (1)$$

where  $(B, \Sigma)$  are parameters and  $(\mathbf{y}_1, \mathbf{x}_1), (\mathbf{y}_2, \mathbf{x}_2), \dots, (\mathbf{y}_n, \mathbf{x}_n)$  are the vector-valued responses and covariates. The number of parameters relative to the sample size in (1) is greater in the multivariate regression model than in its simple linear regression counterpart because the parameters  $(B, \Sigma)$  are matrix-valued [1]. Several methodologies, for example, the lasso and graphical lasso [2], [3], envelope models [4] and reduced rank regression [5], have been proposed to alleviate issues arising from the large number of parameters in (1). However, these methodologies only consider vector-valued observations and do not exploit knowledge of their underlying structure that may further reduce the number of necessary parameters, indeed in some cases making the computation feasible. Here we consider *tensor* or array-structured responses and covariates that arise in psychometrics [6], chemometrics [7], imaging [8], signal processing [9], neuroscience [10] and other applications. We provide two motivating examples next.

### A. Illustrative Examples

1) *Cerebral activity in suicide at-risk subjects*: The United States Center for Disease Control and Prevention reports that 47,173 Americans died in 2017 by suicide, accounting for about two-thirds of all homicides in that year. Accurate suicide risk assessment is challenging, even for trained mental health professionals, as 78% of patients who commit suicide deny such ideation even in their last communication with professionals [11]. Understanding how suicidal subjects respond to different stimuli is important to provide treatment guidance. [12] provided data from a functional Magnetic Resonance images (fMRI) study of nine suicide attempters and eight suicide non-attempter ideators (henceforth, ideators) upon exposing them to 10 words each having positive, negative or death-related connotations. Our interest is in understanding brain regions associated with the interaction of a subject's attempter/ideator status and word type to inform diagnosis and treatment.

Traditional approaches fit separate regression models at each voxel without regard to spatial context which is only addressed in a post-hoc fashion at the time of inference. A more holistic strategy would use (1) with the response vector  $\mathbf{y}_i$  of size  $30 \times 43 \times 56 \times 20 = 1,444,800$ , which contains 30 image volumes of size  $43 \times 56 \times 20$ , for each of the  $i = 1, 2, \dots, 17$  subjects. The explanatory variable here is a two-dimensional (2D) vector that indicates a subject's status as a suicide attempter or ideator. Under this framework,  $B$  has 2,889,600 unconstrained parameters and  $\Sigma$  is a symmetric matrix of 1,043,724,242,400 such parameters, making estimation impractical with only 17 subjects. Incorporating a three-dimensional (3D) spatial autoregressive (AR) structure into the image volume and another correlation structure between the words can ameliorate computational complexity but yields a fourth-order tensor-variate response and a fifth-order tensor-structured parameter  $B$ , analysis of which requires additional methodology. We return to this dataset in Section V-A.

2) *Distinguishing characteristics of faces*: Distinguishing the visual characteristics of faces is important for biometrics and face recognition. The Labeled Faces in the Wild (LFW) database [13] is an useful resource for developing and testing facial recognition methods. This database contains over 13,000  $250 \times 250$  color images of faces of different individuals along with their classification into ethnic origin, age group and gender [14], [15]. We use a subset of only 605 images for which the three attributes of ethnic origin (African, Caucasian or East-Asian, as per the database), cohort (child, youth, middle-aged or senior) and gender (male or female) are non-ambiguous. The colour at each pixel is a 3D RGB vector so each image (response) is a  $250 \times 250 \times 3$  three-way array. Each of the three image attributes can be represented by an indicator vector so that we get a three-way tensor-variate structure for the covariates (attributes). Our objective is to train a linear model to help us distinguish the visual characteristics of different attributes. Transforming the 3D tensors into long vectors and fitting (1) requires a  $B$  of  $250 \times 250 \times 3 \times 2 \times 3 \times 4 = 4,500,000$  unconstrained parameters and an error covariance matrix  $\Sigma$  of over 17 billion similar parameters, making accurate inference (from only 605 observed images) impractical. Methodology that incorporates the reductions afforded by the tensor-variate structures of the responses and the covariates can redeem the situation. We revisit this dataset in Section V-B.

## B. Overview of the Paper

The previous examples show the inadequacy of training (1) on tensor-valued data, without additional accommodation for structure, as the sizes of  $B$  and  $\Sigma$ , in unconstrained vector-variate regression, grow with the dimensions of the tensor-valued responses and explanatory variables. In this paper, we study (1) for tensor-valued responses and covariates, and propose a general framework to simultaneously reduce the number of unconstrained parameters in  $B$  and  $\Sigma$ . For  $B$  we investigate four types of low-rank structures: the *canonical polyadic* (CP) [16], [17], the Tucker [18], [19], the tensor ring (TR) [20], [21] and the outer matrix product (OP) formats, that we introduce here. The error in (1) is modeled by the *tensor-variate normal* (TVN) distribution [22]–[25] that posits the  $\Sigma$  of (1) to be the Kronecker product of multiple matrices. We develop methodology for tensor-on-tensor regression and tensor-variate analysis of variance (TANOVA) under this framework.

The rest of the paper is structured as follows. Section II presents notations and network diagrams, low-rank tensor formats, the TVN distribution and preliminary results that we develop for use in this paper. Section III formulates tensor-on-tensor regression and TANOVA methodology with low-rank tensor formats on  $\mathcal{B}$  and tensor normal errors. We develop algorithms for finding maximum likelihood (ML) estimators and derive their asymptotic distributions. We evaluate performance of our methods in two simulation scenarios in Section IV. Section V applies our developed methodology to the datasets of Sections I-A1 and I-A2. We conclude with some discussion. An online supplement with sections, theorems, lemmas, figures and equations prefixed with “S” is also available.

## II. BACKGROUND AND PRELIMINARY DEVELOPMENT

This section provides a unified treatment of tensor reshapings and contractions following the notation of [26], [19], and [27]. We denote the trace using  $\text{tr}(\cdot)$ , the transpose using  $(\cdot)'$ , the pseudo-inverse using  $(\cdot)^{-}$ , the identity matrix of size  $n \times n$  using  $I_n$  and the Kronecker product using  $\otimes$  (see Section S1 for additional definitions and illustrations). We define tensors as multi-dimensional arrays of numbers. The total number of *modes* or sides of a tensor is called its *order*. Inspired by the notation in [27] and [19] we refer to scalars using lower-case letters (*i.e.*  $x$ ), vectors using bold lower-case italicized letters (*i.e.*  $\mathbf{x}$ ), matrices using upper-case letters (*i.e.*  $X$ ), and higher-order tensors using a calligraphic script (*i.e.*  $\mathcal{X}$ ). Random arrays of any order are denoted using bold capital letters (*i.e.*  $\mathbf{X}$ ). We denote the  $(i_1, i_2, \dots, i_p)$ th element of a tensor  $\mathcal{X}$  using  $\mathcal{X}(i_1, i_2, \dots, i_p)$ . The vector outer product (with notation  $\circ$ ) of  $p$  vectors generates the  $p$ th-order tensor  $\mathcal{X} = \circ_{j=1}^p \mathbf{x}_j$  with  $(i_1, i_2, \dots, i_p)$ th element  $\mathcal{X}(i_1, i_2, \dots, i_p) = \prod_{j=1}^p \mathbf{x}_j(i_j)$ . Any  $p$ th-order tensor  $\mathcal{X} \in \mathbb{R}^{m_1 \times m_2 \times \dots \times m_p}$  can be expressed using the vector outer product as

$$\mathcal{X} = \sum_{i_1=1}^{m_1} \dots \sum_{i_p=1}^{m_p} \mathcal{X}(i_1, \dots, i_p) \left( \bigcirc_{q=1}^p \mathbf{e}_{i_q}^{m_q} \right), \quad (2)$$

where  $\mathbf{e}_i^m \in \mathbb{R}^m$  is a unit basis vector with 1 as the  $i$ th element and 0 everywhere else. Equation (2) allows us to reshape a tensor by only manipulating the vector outer product. A  $p$ th-order diagonal tensor  $\mathbb{I}_r^p \in \mathbb{R}^{r \times r \times \dots \times r}$  has zeroes everywhere but for when the indices in each mode coincide, where it is unity. Formally

$$\mathbb{I}_r^p = \sum_{i=1}^r \left( \bigcirc_{q=1}^p \mathbf{e}_i^r \right). \quad (3)$$

Tensor structures may be conveniently represented by tensor network diagrams that are a recent adaptation [27] from quantum physics where they were originally introduced to visually describe many-body problems. Each node in a tensor network diagram corresponds to a tensor and the number of edges coming from the node represents a mode. A node with no edges is a scalar, a node with one edge is a vector, a node with two edges is a matrix and a node with  $p$  edges is a  $p$ th-order tensor (see Figures 1a–1d). (The angle between edges has no meaning beyond aesthetics.) Diagonal tensors as in (3) are represented by putting a diagonal across the node, as in Figure 1d.

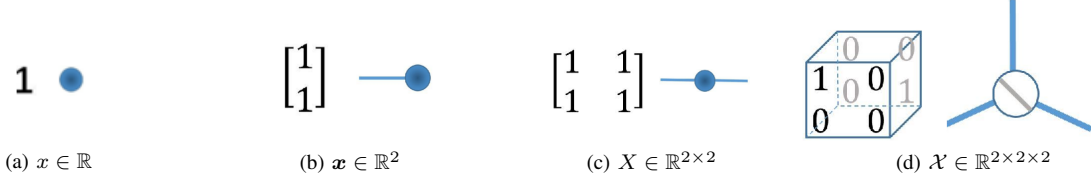


Fig. 1: Tensor network diagrams of a (a) scalar, (b) vector, (c) matrix and (d) third-order diagonal tensor.

TABLE I: Tensor reshapings defined by specifying partitions  $(\mathcal{S}, \mathcal{T})$  of  $\mathcal{M}$  in equation (4).

Reshaping	Notation	$\mathcal{S}$	$\mathcal{T}$
$k$ th mode matricization	$\mathcal{X}_{(k)}$	$\{k\}$	$\{1, 2, \dots, k-1, k+1, k+2, \dots, p\}$
$k$ th canonical matricization	$\mathcal{X}_{<k>}$	$\{1, 2, \dots, k\}$	$\{k+1, k+2, \dots, p\}$
vectorization	$\text{vec}(\mathcal{X})$	$\{1, 2, \dots, p\}$	$\emptyset$

#### A. Tensor reshapings, contractions and low-rank formats

The matricization of a tensor is a matrix with its elements arranged differently. The following definition is from [26]

**Definition II.1.** Let  $\mathcal{S} = \{r_1, r_2, \dots, r_L\}$  and  $\mathcal{T} = \{m_1, m_2, \dots, m_M\}$  be ordered sets that partition the set of modes  $\mathcal{M} = \{1, 2, \dots, p\}$  of  $\mathcal{X} \in \mathbb{R}^{m_1 \times m_2 \times \dots \times m_p}$ . Here  $L + M = p$ . Then the matricization  $\mathcal{X}_{(\mathcal{S} \times \mathcal{T})}$  is a matrix of size  $(\prod_{q \in \mathcal{S}} m_q) \times (\prod_{q \in \mathcal{T}} m_q)$  defined as

$$\mathcal{X}_{(\mathcal{S} \times \mathcal{T})} = \sum_{i_1=1}^{m_1} \dots \sum_{i_p=1}^{m_p} \mathcal{X}(i_1, i_2, \dots, i_p) \left( \bigotimes_{q \in \mathcal{S}} e_{i_q}^{m_q} \right) \left( \bigotimes_{q \in \mathcal{T}} e_{i_q}^{m_q} \right)'. \quad (4)$$

We define matricizations in *reverse lexicographic* order to be consistent with the traditional matrix vectorization. This means that the  $q$  modes in the multiple Kronecker product (4) are selected in reverse order. Table I defines several reshapings by selecting different partitions  $(\mathcal{S}, \mathcal{T})$  of  $\mathcal{M}$ . These definitions are individually clarified in Equations (S3), (S4) and (S5).

Tensor contractions [27] generalize the matrix product to higher-ordered-tensors. We use  $\mathcal{X} \times_{k_1, l_2, \dots, l_a}^{l_1, l_2, \dots, l_a} \mathcal{Y}$  to denote the mode- $\binom{l_1, l_2, \dots, l_a}{k_1, k_2, \dots, k_a}$  product or contraction between the  $(k_1, k_2, \dots, k_a)$  modes of  $\mathcal{X} \in \mathbb{R}^{m_1 \times m_2 \times \dots \times m_p}$  and the  $(l_1, l_2, \dots, l_a)$  modes of  $\mathcal{Y} \in \mathbb{R}^{n_1 \times n_2 \times \dots \times n_q}$ , where  $m_{k_1} = n_{l_1}, m_{k_2} = n_{l_2}, \dots, m_{k_a} = n_{l_a}$ . This contraction results in a tensor of order  $p + q - 2a$  where the  $a$  pairs of modes  $(l_j, k_j)$  get *contracted*. A simple contraction between the  $k$ th mode of  $\mathcal{X}$  and the  $l$ th mode of  $\mathcal{Y}$ , where  $m_k = n_l$ , has  $(i_1, i_2, \dots, i_{k-1}, i_{k+1}, \dots, i_p, j_1, j_2, \dots, j_{l-1}, j_{l+1}, \dots, j_q)$ th element

$$\sum_{t=1}^{m_l} \mathcal{X}(i_1, i_2, \dots, i_{k-1}, t, i_{k+1}, \dots, i_p) \mathcal{Y}(j_1, j_2, \dots, j_{l-1}, t, j_{l+1}, \dots, j_q). \quad (5)$$

Similarly, multiple contractions sum over multiple products of the elements of  $\mathcal{X}$  and  $\mathcal{Y}$ . Table II defines some contractions with this notation. An important special case is the partial contraction that contracts all the  $p < q$  modes of  $\mathcal{X} \in \mathbb{R}^{m_1 \times \dots \times m_p}$  with the first  $p$  modes of  $\mathcal{Y} \in \mathbb{R}^{m_1 \times \dots \times m_q}$  resulting in a tensor  $\langle \mathcal{X} | \mathcal{Y} \rangle = \mathcal{X} \times_{1, \dots, p}^{1, \dots, p} \mathcal{Y}$  of size  $\mathbb{R}^{m_{p+1} \times \dots \times m_q}$ . The partial contraction helps define tensor-on-tensor regression, and can also be written as a matrix-vector multiplication using Lemma II.15 (below). The tensor trace is a self-contraction between the two outer-most modes of a tensor. If  $m_1 = m_p$ , then

$$\text{tr}(\mathcal{X}) = \sum_{i=1}^{m_1} \mathcal{X}(i, :, \dots, :, i), \quad (6)$$

TABLE II: Tensor contractions, where the contraction along one mode is defined as per (5). Here  $\mathcal{X} \in \mathbb{R}^{m_1 \times m_2 \times \dots \times m_p}$ ,  $\mathcal{Y} \in \mathbb{R}^{n_1 \times n_2 \times \dots \times n_q}$ , and  $X$  and  $Y$  are the cases where  $p = 2$  and  $q = 2$  respectively.

Contraction	Notation	Definition	Conditions
matrix product	$XY$	$X \times_{\frac{1}{2}}^{\frac{1}{2}} Y$	$p = q = 2$
$k$ th mode matrix product	$\mathcal{X} \times_k Y$	$\mathcal{X} \times_k^2 Y$	$q = 2$
$k$ th mode vector product	$\mathcal{X} \bar{\times}_k \mathbf{y}$	$\mathcal{X} \times_k^1 \mathbf{y}$	$q = 1$
inner product	$\langle \mathcal{X}, \mathcal{Y} \rangle$	$\mathcal{X} \times_{1, 2, \dots, p}^{1, 2, \dots, q} \mathcal{Y}$	$p = q$
partial contraction	$\langle \mathcal{X}   \mathcal{Y} \rangle$	$\mathcal{X} \times_{1, \dots, p}^{1, \dots, p} \mathcal{Y}$	$p < q$
last mode with first mode	$\mathcal{X} \times^1 \mathcal{Y}$	$\mathcal{X} \times_p^1 \mathcal{Y}$	—

where  $\text{tr}(\mathcal{X}) \in \mathbb{R}^{m_2 \times m_3 \times \dots \times m_{p-1}}$ . The contraction between two distinct modes (from possibly the same tensor) is represented in tensor network diagrams by joining the corresponding edges (see Figure 2 for examples). Also, applying the  $k$ th mode

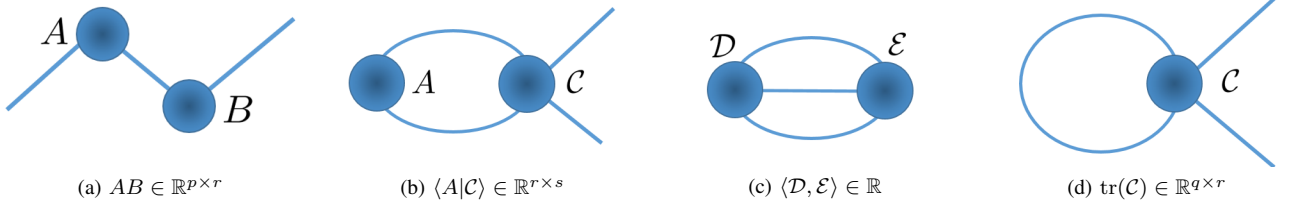


Fig. 2: Tensor network diagrams of example (a) matrix product, (b) partial contraction, (c) inner product and (d) trace. Here  $A \in \mathbb{R}^{p \times q}$ ,  $B \in \mathbb{R}^{q \times r}$ ,  $D, E \in \mathbb{R}^{p \times q \times r}$  and  $C \in \mathbb{R}^{p \times q \times r \times p}$ .

matricization to every mode of  $\mathcal{V} \in \mathbb{R}^{g_1 \times g_2 \times \dots \times g_p}$  with respect to  $A_i \in \mathbb{R}^{m_i \times g_i}$ ,  $i = 1, 2, \dots, p$  results in the Tucker product

$$\mathcal{B} = \llbracket \mathcal{V}; A_1, \dots, A_p \rrbracket = \mathcal{V} \times_1 A_1 \times_2 \dots \times_p A_p = \sum_{i_1=1}^{m_1} \dots \sum_{i_p=1}^{m_p} \mathcal{V}(i_1 \dots i_p) \left( \begin{smallmatrix} p \\ q=1 \end{smallmatrix} A_q(:, i_q) \right). \quad (7)$$

A tensor  $\mathcal{B}$  that can be written as the product in (7) is said to have a Tucker format with Tucker rank  $(g_1, g_2, \dots, g_p)$ . In this case  $\mathcal{V}$  is called the *core tensor* and  $A_1, A_2, \dots, A_p$  are the *factor matrices*. When  $g_i < m_i$  for  $i = 1, 2, \dots, p$ , the Tucker format substantially reduces the number of unconstrained elements in a tensor and its complexity. Tucker formats are often fit by a higher-order singular value decomposition (HOSVD) [28] or higher-order LQ decomposition (HOLQ) [29]. For a diagonal core tensor  $\mathcal{V}$ , as in (3), the Tucker format reduces to the CP format of rank  $r$ . This reduction is equivalent to setting the tensor  $\mathcal{B}$  as the sum of  $r$  vector outer products, where the vectors correspond to the columns of matrix factors  $A_i \in \mathbb{R}^{m_i \times r}$ ,  $i = 1, \dots, p$ ,

$$\mathcal{B} = \llbracket \boldsymbol{\lambda}; A_1, \dots, A_p \rrbracket = \sum_{i=1}^r \boldsymbol{\lambda}(i) \left( \begin{smallmatrix} p \\ q=1 \end{smallmatrix} A_q(:, i) \right). \quad (8)$$

The vector  $\boldsymbol{\lambda} \in \mathbb{R}^r$  contains the diagonal entries of the core tensor, and is often set to the proportionality constants that make the matrix factors have unit column norms. When  $\boldsymbol{\lambda}$  is ignored in the specification of (8), we assume that  $\boldsymbol{\lambda} = [1, 1, \dots, 1]'$ .

A tensor  $\mathcal{B}$  is said to have an Outer Product (OP) format if it can be written as

$$\mathcal{B} = \circ \llbracket M_1, M_2, \dots, M_p \rrbracket = \sum_{i_1=1}^{m_1} \sum_{j_1=1}^{h_1} \dots \sum_{i_p=1}^{m_p} \sum_{j_p=1}^{h_p} \left( \prod_{q=1}^p M_q[i_q, j_q] \right) \left\{ \left( \begin{smallmatrix} p \\ q=1 \end{smallmatrix} \mathbf{e}_{j_q}^{h_q} \right) \circ \left( \begin{smallmatrix} p \\ q=1 \end{smallmatrix} \mathbf{e}_{i_q}^{m_q} \right) \right\}. \quad (9)$$

The OP format of (9) is the outer product of multiple matrices, and it is useful for expressing the Tucker product of (7) as a partial contraction between  $\mathcal{V}$  and  $\circ \llbracket A_1, A_2, \dots, A_p \rrbracket$ , as we shortly state and prove in Theorem II.1b. The derivation needs some properties of tensor products and reshaping that we prove first.

**Lemma II.1.** Let  $\mathcal{X} \in \mathbb{R}^{m_1 \times m_2 \times \dots \times m_p}$ . Then using the notation of Tables I and II,

- 1)  $\mathcal{X}_{\langle p-1 \rangle} = \mathcal{X}'_{(p)}$ .
- 2)  $\text{vec}(\mathcal{X}) = \text{vec}(\mathcal{X}_{(1)}) = \text{vec}(\mathcal{X}_{\langle 1 \rangle}) = \text{vec}(\mathcal{X}_{\langle 2 \rangle}) = \dots = \text{vec}(\mathcal{X}_{\langle p \rangle})$ .
- 3)  $\langle \mathcal{X}, \mathcal{Y} \rangle = (\text{vec} \mathcal{X})' (\text{vec} \mathcal{Y}) = \text{tr}(\mathcal{X}_{(k)} \mathcal{Y}'_{(k)})$ ,  $\mathcal{Y} \in \mathbb{R}^{m_1 \times m_2 \times \dots \times m_p}$ ,  $k = 1, \dots, p$ .
- 4)  $\text{vec} \llbracket \mathcal{X}; A_1, \dots, A_p \rrbracket = \left( \bigotimes_{i=p}^1 A_i \right) \text{vec}(\mathcal{X})$ , where  $A_i \in \mathbb{R}^{n_i \times m_i}$  for any  $n_i \in \mathbb{N}$ .
- 5)  $\text{vec} \langle \mathcal{X} | \mathcal{B} \rangle = \mathcal{B}'_{\langle p \rangle} \text{vec} \mathcal{X}$ ,  $\mathcal{B} \in \mathbb{R}^{m_1 \times m_2 \times \dots \times m_p \times h_1 \times h_2 \times \dots \times h_p}$ ,  $q \in \mathbb{N}$ .
- 6)  $\text{vec}(\mathcal{X}_{(k)}) = K_{(k)} \text{vec}(\mathcal{X})$ ,  $K_{(k)} = (I_{\prod_{i=k+1}^p m_i} \otimes K_{\prod_{i=1}^{k-1} m_i, m_k})$ ,  $k = 1, 2, \dots, p$ .

*Proof.* See Section S1-C. □

We are now ready to state and prove

**Theorem II.1.** Consider the  $p$ th-order tensor  $\mathcal{X}$  and the matrices  $M_1, M_2, \dots, M_p$  such that the Tucker product with  $\mathcal{X}$  can be formed. Then

- 1)  $\circ \llbracket M_1, M_2, \dots, M_p \rrbracket_{\langle p \rangle} = \bigotimes_{q=p}^1 M'_q$ .
- 2)  $\langle \mathcal{X} | \circ \llbracket M_1, M_2, \dots, M_p \rrbracket \rangle = \llbracket \mathcal{X}; M_1, M_2, \dots, M_p \rrbracket$ .
- 3) For any  $k = 1, 2, \dots, p$ , let  $\mathcal{S} = \{k, p+k\}$ . Then

$$\circ \llbracket M_1, M_2, \dots, M_p \rrbracket_{(\mathcal{S} \times \mathcal{S}^c)} = (\text{vec} M'_k)' (\text{vec} \circ \llbracket M_1, M_2, \dots, M_{k-1}, M_{k+1}, \dots, M_p \rrbracket). \quad (10)$$

*Proof.* See Section S1-D. □

a) *Remark:* If  $\mathcal{B} = \circ[[X', X']]$  for some matrix  $X$ , then Theorem II.1(1) implies that  $\mathcal{B}_{\langle 2 \rangle} = X \otimes X$  while  $\mathcal{B}_{(1,3) \times (2,4)} = (\text{vec } X)(\text{vec } X)'$  by Theorem II.1(3). In other words,  $X \otimes X$  and  $(\text{vec } X)(\text{vec } X)'$  are different matricizations of the same OP tensor  $\mathcal{B}$ . This reformulation formalizes our intuition because both  $X \otimes X$  and  $(\text{vec } X)(\text{vec } X)'$  have the same number of elements, and it motivates naming the format *outer product*.

Finally, a tensor  $\mathcal{B}$  is said to have a Tensor Ring (TR) format with TR rank  $(g_1, g_2, \dots, g_p)$  if it can be expressed as

$$\mathcal{B} = \text{tr}(\mathcal{G}_1 \times^1 \mathcal{G}_2 \times^1 \dots \times^1 \mathcal{G}_p), \quad (11)$$

where  $\mathcal{G}_i \in \mathbb{R}^{g_{i-1} \times m_i \times g_i}$  for  $i = 1, \dots, p$  and  $g_0 = g_p$ . The TR format is called the Matrix Product State (MPS) with closed boundary conditions in many-body physics [30]. When exactly one of the TR ranks is 1, the TR format is the same as the Tensor Train (TT) format [21] and is the MPS with open boundary conditions.

We conclude our discussion of low-rank tensor formats by illustrating, in Figure 3, tensor network diagrams of a fourth-order tensor in the Tucker, CP, OP and TR formats.

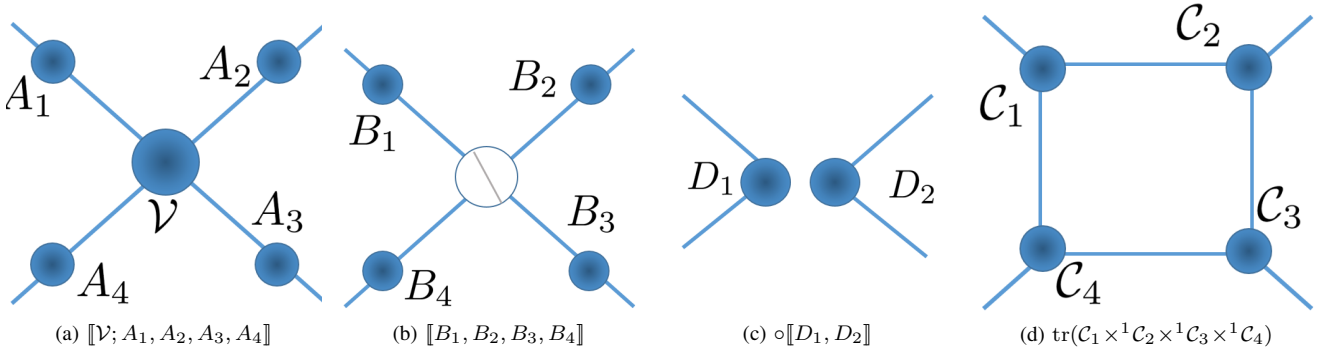


Fig. 3: Tensor network diagrams of an example fourth-order tensor having the (a) Tucker format of (7), (b) CP format of (8), (c) OP format of (9) and (d) TR format of (11). (The matrix outer product in (c) is displayed by having nodes of  $D_1$  and  $D_2$  close, but not connected, to each other, yielding a 4th-order tensor with the combined dimensions of  $D_1$  and  $D_2$ ).

### B. The TVN Distribution

The matrix-variate normal distribution, abbreviated in [31] as MxVN to distinguish it from the vector-variate multinormal distribution (MVN), was studied extensively in [32]. A random matrix  $\mathbf{X} \in \mathbb{R}^{m_1 \times m_2}$  follows a MxVN distribution if  $\text{vec}(\mathbf{X})$  is MVN with covariance matrix  $\Sigma_2 \otimes \Sigma_1$ , where  $\Sigma_k \in \mathbb{R}^{m_k \times m_k}$  for  $k = 1, 2$ . Our TVN distribution, formulated in Definition II.2, extends this idea to the case of higher-order random tensors.

**Definition II.2.** A random tensor  $\mathbf{X} \in \mathbb{R}^{m_1 \times m_2 \times \dots \times m_p}$  follows a  $p$ th-order TVN distribution with mean  $\mathcal{M} \in \mathbb{R}^{m_1 \times m_2 \times \dots \times m_p}$  and non-negative definite scale matrices  $\Sigma_i \in \mathbb{R}^{m_i \times m_i}$  for  $i = 1, 2, \dots, p$  (that is,  $\mathbf{X} \sim \mathcal{N}_{m_1, m_2, \dots, m_p}(\mathcal{M}, \Sigma_1, \Sigma_2, \dots, \Sigma_p)$ ) if and only if  $\text{vec}(\mathbf{X}) \sim \mathcal{N}_{m_1 \times m_2 \times \dots \times m_p}(\text{vec}(\mathcal{M}), \bigotimes_{i=1}^p \Sigma_i)$ .

The Kronecker product in Definition II.2 is in reverse order because we defined vectorization of a tensor in reverse lexicographic order. For simplicity, we use the following notation for the rest of the paper

$$m = \prod_{i=1}^p m_i, \quad m_{-k} = \prod_{i=1, i \neq k}^p m_i, \quad \Sigma = \bigotimes_{i=p}^1 \Sigma_i, \quad \Sigma_{-k} = \bigotimes_{i=p, i \neq k}^1 \Sigma_i.$$

Definition II.2 defines the TVN distribution in terms of a vectorization. We state and prove the distribution of other tensor reshapings in Theorem II.2. These results are essential in the development of tensor-on-tensor regression models with TVN errors, as they allow us to model the vectorized tensor errors in terms of the MVN distribution.

**Theorem II.2.** The following statements are equivalent:

- 1)  $\mathbf{Y} \sim \mathcal{N}_{m_1, m_2, \dots, m_p}(\mathcal{M}, \Sigma_1, \Sigma_2, \dots, \Sigma_p)$
- 2)  $\text{vec}(\mathbf{Y}) \sim \mathcal{N}_m(\text{vec}(\mathcal{M}), \Sigma)$
- 3)  $\mathbf{Y}_{(k)} \sim \mathcal{N}_{m_k, m_{-k}}(\mathcal{M}_{(k)}, \Sigma_k, \Sigma_{-k}), \quad k = 1, 2, \dots, p$
- 4)  $\mathbf{Y}_{\langle k \rangle} \sim \mathcal{N}_{\prod_{i=1}^k m_i, \prod_{i=k+1}^p m_i}(\mathcal{M}_{\langle k \rangle}, \bigotimes_{i=k}^1 \Sigma_i, \bigotimes_{i=p}^{k+1} \Sigma_i), \quad k = 1, 2, \dots, p$

*Proof.* The equivalence of (a) and (b) is from Definition II.2. The equivalence of (b) and (c) arises from Lemma II.1(6), which states that  $\text{vec}(\mathbf{Y}_{(k)}) = K_{(k)} \text{vec}(\mathbf{Y})$ , where  $K_{(k)} \Sigma K_{(k)}' = \Sigma_{-k} \otimes \Sigma_k$ . Finally, (b) and (d) are equivalent, following Lemma II.1(2) that states that  $\text{vec}(\mathbf{Y}_{\langle k \rangle}) = \text{vec}(\mathbf{Y})$ .  $\square$   $\square$

The pdf of  $\mathbf{Y} \sim \mathcal{N}_{m_1, m_2, \dots, m_p}(\mathcal{M}, \Sigma_1, \Sigma_2, \dots, \Sigma_p)$  is

$$f(\mathbf{Y} = \mathcal{Y}; \mathcal{M}, \Sigma_1, \Sigma_2, \dots, \Sigma_p) = (2\pi)^{-m/2} |\Sigma|^{-1/2} \exp \left\{ -\frac{1}{2} D_{\Sigma}^2(\mathcal{Y}, \mathcal{M}) \right\}, \quad (12)$$

where  $\Sigma$  is as in Definition II-B and the squared Mahalanobis distance  $D_{\Sigma}^2(\mathcal{Y}, \mathcal{M})$  between  $\mathcal{Y}$  and  $\mathcal{M}$  has the following equivalent representations, because of Lemmas II.1(3) and II.1(4)

$$D_{\Sigma}^2(\mathcal{Y}, \mathcal{M}) = \text{vec}(\mathcal{Y} - \mathcal{M})' \Sigma^{-1} \text{vec}(\mathcal{Y} - \mathcal{M}) \quad (13)$$

$$= \text{tr} \left[ \Sigma_k^{-1} (\mathcal{Y} - \mathcal{M})'_{(k)} \Sigma_{-k}^{-1} (\mathcal{Y} - \mathcal{M})_{(k)} \right], \quad k = 1, 2, \dots, p \quad (14)$$

$$= \langle (\mathcal{Y} - \mathcal{M}), [(\mathcal{Y} - \mathcal{M}); \Sigma_1^{-1}, \Sigma_2^{-1}, \dots, \Sigma_p^{-1}] \rangle. \quad (15)$$

See Properties S1.2 for similar alternative expressions for the determinant  $\det(\Sigma)$  of  $\Sigma$ . We now describe the distribution of the Tucker product of a random TVN tensor.

**Lemma II.2.** *If  $\mathbf{Y} \sim \mathcal{N}_{m_1, m_2, \dots, m_p}(0, \Sigma_1, \Sigma_2, \dots, \Sigma_p)$  and  $M_k \in \mathbb{R}^{n_k \times m_k}$  for all  $k = 1, 2, \dots, p$ , then  $\mathbf{X} = [\mathbf{Y}; M_1, M_2, \dots, M_p] \sim \mathcal{N}_{n_1, n_2, \dots, n_p}(0, M_1 \Sigma_1 M_1', M_2 \Sigma_2 M_2', \dots, M_p \Sigma_p M_p')$ .*

*Proof.* From Lemma II.1(4) and properties of the MVN distribution,

$$\text{vec}(\mathbf{X}) = \left( \bigotimes_{k=p}^1 M_k \right) \text{vec}(\mathbf{Y}) \sim \mathcal{N}_{n_1 \times \dots \times n_p} \left( 0, \left( \bigotimes_{k=p}^1 M_k \right) \left( \bigotimes_{k=p}^1 \Sigma_k \right) \left( \bigotimes_{k=p}^1 M_k \right)' \right).$$

The remainder of the proof follows from Property S1.2(d) and Definition II.2.  $\square$   $\square$

### III. METHODOLOGY

This section introduces a regression model with TVN errors and tensor-valued responses and covariates. A special case of the regression setup leads us to a tensor-variate analogue of the Analysis of Variance (ANOVA) that we call TANOVA. We develop algorithms for ML estimation under the Tucker, CP, OP and TR low-rank formats and provide asymptotic properties of our estimators.

#### A. Tensor-variate Linear Models with TVN Errors

1) *Tensor-on-Tensor Regression:* We formulate the tensor-on-tensor regression model as

$$\mathcal{Y}_i = \Upsilon + \langle \mathcal{X}_i | \mathcal{B} \rangle + \mathcal{E}_i, \quad \mathcal{E}_i \stackrel{iid}{\sim} \mathcal{N}_{m_1, m_2, \dots, m_p}(0, \sigma^2 \Sigma_1, \Sigma_2, \dots, \Sigma_p), \quad i = 1, 2, \dots, n, \quad (16)$$

where  $\mathcal{Y}_i \in \mathbb{R}^{m_1 \times m_2 \times \dots \times m_p}$  is the tensor-valued response,  $\mathcal{X}_i \in \mathbb{R}^{h_1 \times h_2 \times \dots \times h_l}$  the tensor-valued covariate,  $\mathcal{B} \in \mathbb{R}^{h_1 \times h_2 \times \dots \times h_l \times m_1 \times m_2 \times \dots \times m_p}$  is the (tensor-valued) regression parameter and  $\Upsilon$  is the (tensor-valued) intercept. This model is essentially the classical multivariate multiple linear regression (MVMLR) model but exploits the tensor-valued structure of the covariates and responses to reduce the total number of parameters. To see this, we apply Lemma II.1(5) along with Theorem II.2(2) to vectorize (16) as

$$\text{vec}(\mathcal{Y}_i) = \text{vec}(\Upsilon) + \mathcal{B}'_{<I>} \text{vec}(\mathcal{X}_i) + \mathbf{e}_i, \quad \mathbf{e}_i \stackrel{iid}{\sim} \mathcal{N}_{m_1 \times \dots \times m_p}(0, \sigma^2 \Sigma), \quad (17)$$

which yields a MVMLR model with intercept. As in MVMLR, the intercept term in (17) can be incorporated into the covariates as  $[\text{vec}(\Upsilon) \mathcal{B}'_{<I>}] [1, \text{vec}(\mathcal{X}_i)']'$ , however the covariate  $[1, \text{vec}(\mathcal{X}_i)']'$  is then no longer a vectorized tensor and we cannot exploit the tensor structure of  $\mathcal{X}_i$ . To obviate this possibility, (16) includes a separate intercept term  $\Upsilon$ .

Imposing a low-rank format on  $\mathcal{B}$  proffers several advantages. First, it makes the regression model practical to use, as accurate estimation of an unstructured version of  $\mathcal{B}$  may otherwise be prohibitive when dimensionality is high relative to sample size. Second,  $\mathcal{B}$  can be interpreted, in spite of its high dimensions, as being explainable through a few lower-dimensional tensor factor matrices (Figure 4). These explanations mirror the many-body problem in physics, where weakly-coupled degrees of freedom are often embedded in ultra-high-dimensional Hilbert spaces [30], [33]. We now turn to the problem of learning  $\mathcal{B}$  in the given setup.

The TVN distribution of the  $\mathcal{E}_i$ s in (16) leads to a Kronecker-separable dispersion matrix  $\Sigma$ , reducing the number of unconstrained parameters from  $(\prod_{i=1}^p m_i) \times (\prod_{i=1}^p m_i + 1)/2$  to  $\sum_{i=1}^p m_i(m_i + 1)/2$ . Kronecker separability results in unidentifiable scale matrices  $(\Sigma_i)$ , as  $cA \otimes B = A \otimes cB$  for any matrices  $A, B$  and non-zero scalar  $c$ . Therefore, for identifiability, we constrain the scale matrices to have  $\Sigma_i(1, 1) = 1$  while introducing a parameter  $\sigma^2$  that captures an overall proportional scalar variance. This approach further reduces the number of parameters by  $p - 1$  and imposes a curved exponential family distribution on the errors [34].

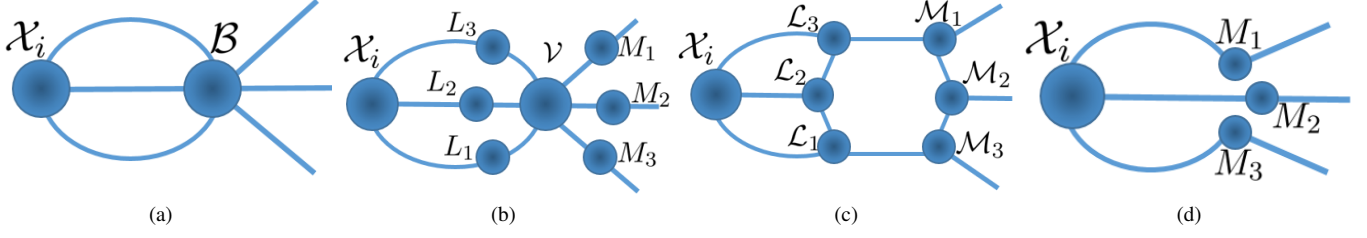


Fig. 4: Tensor network diagrams of tensor-on-tensor regression when both the response and the covariates are third-order tensors and for (a)  $\mathcal{Y}_i = \langle \mathcal{X}_i | \mathcal{B} \rangle$  and (b-d) the special cases when the  $\mathcal{B}$  in  $\langle \mathcal{X}_i | \mathcal{B} \rangle$  are of (b) Tucker, (c) TR and (d) OP formats (illustrated in Figure 3).

2) *The TANOVA model:* Suppose that we observe independent tensors  $\mathcal{Y}_{j_1, j_2, \dots, j_l, i}$ ,  $i = 1, 2, \dots, n_{j_1, j_2, \dots, j_l}$ , each of size  $m_1 \times m_2 \times \dots \times m_p$ , where  $j_k$ ,  $k = 1, 2, \dots, l$ , indexes the  $k$ th categorical (factor) variable of  $h_k$  levels, that is,  $j_k \in \{1, 2, \dots, h_k\}$ . The tensor-valued parameter  $\mathcal{B}$  encoding the dimensions of  $\mathcal{Y}_{i, j_1, j_2, \dots, j_l}$  and all the possible factor classes is of size  $h_1 \times h_2 \times \dots \times h_l \times m_1 \times m_2 \times \dots \times m_p$ . To see this, consider the  $l$ th ordered single-entry tensor  $\mathcal{X}_{j_1, j_2, \dots, j_l} = \bigcirc_{q=1}^l e_{i_q}^{h_q}$  that is unity at  $(j_1, j_2, \dots, j_l)$  and zero everywhere else. Then

$$\langle \mathcal{X}_{j_1, j_2, \dots, j_l} | \mathcal{B} \rangle = \mathcal{B}[j_1, j_2, \dots, j_l, :, :, \dots, :] \in \mathbb{R}^{m_1 \times m_2 \times \dots \times m_p}. \quad (18)$$

Therefore, modeling  $\mathbb{E}(\mathcal{Y}_{i, j_1, j_2, \dots, j_l})$  as  $\langle \mathcal{X}_{j_1, j_2, \dots, j_l} | \mathcal{B} \rangle$  results in each factor combination  $(j_1, j_2, \dots, j_p)$  getting assigned its own mean parameter as a sub-tensor of  $\mathcal{B}$ . This high-dimensional parameter  $\mathcal{B}$  is identical to the cell-means multivariate ANOVA (MANOVA) if we vectorize (18) using Lemma II.1(5) as

$$\mathcal{B}'_{<l>} \text{vec}(\mathcal{X}_{j_1, j_2, \dots, j_l}) = \text{vec}(\mathcal{B}[j_1, j_2, \dots, j_p, :, :, \dots, :]), \quad (19)$$

in which case  $\text{vec}(\mathcal{X}_{j_1, j_2, \dots, j_p}) = \bigotimes_{q=1}^p e_{i_q}^{h_q}$  corresponds to a row in the MANOVA design matrix. Although (18) and (19) are fundamentally the same, the formulation in (18) helps us visualize and formulate a low-rank format on  $\mathcal{B}$ . Based on the format, we refer to tensor-valued response regression models with the mean in (18) as TANOVA( $l, p$ ), where  $l$  is the number of different factors and  $p$  is the order of the tensor-valued response. In this way, because scalar and vector variables are tensors of order 0 and 1, ANOVA and MANOVA correspond to TANOVA(1, 0) and TANOVA(1, 1), respectively. In general, the TANOVA( $l, p$ ) model with TVN errors can be expressed as

$$\mathcal{Y}_i = \langle \mathcal{X}_i | \mathcal{B} \rangle + \mathcal{E}_i, \quad \mathcal{E}_i \stackrel{iid}{\sim} \mathcal{N}_{m_1, m_2, \dots, m_p}(0, \sigma^2 \Sigma_1, \Sigma_2, \dots, \Sigma_p), \quad i = 1, 2, \dots, n, \quad (20)$$

where  $\mathcal{X}_i$  is the single-entry tensor that contains all the assigned factors of  $\mathcal{Y}_i$ . Model (20) is a tensor-on-tensor regression model as in (16) with no intercept. This is analogous to ANOVA and MANOVA being special cases of univariate and multivariate multiple linear regressions, respectively. Further, the log-likelihood function of (20) is

$$\ell = -\frac{n}{2} \log |\sigma^2 \Sigma| - \frac{1}{2\sigma^2} \sum_{i=1}^n \langle \mathcal{Y}_i - \langle \mathcal{X}_i | \mathcal{B} \rangle, \llbracket \mathcal{Y}_i - \langle \mathcal{X}_i | \mathcal{B} \rangle; \Sigma_1^{-1}, \Sigma_2^{-1}, \dots, \Sigma_p^{-1} \rrbracket \rangle. \quad (21)$$

### B. Parameter Estimation

We now develop algorithms to estimate (16) for when  $\mathcal{B}$  has four different formats, and study the exact and asymptotic properties of the derived estimators.

1) *Profiling the intercept:* First we show that the intercept in (16) can be profiled out by centering the covariates and the responses. To see this, we use (12) to express the loglikelihood in terms of  $\Upsilon$ :

$$\ell = -\frac{1}{2\sigma^2} \sum_{i=1}^n \langle \mathcal{Y}_i - \Upsilon - \langle \mathcal{X}_i | \mathcal{B} \rangle, \llbracket \mathcal{Y}_i - \Upsilon - \langle \mathcal{X}_i | \mathcal{B} \rangle; \Sigma_1^{-1}, \Sigma_2^{-1}, \dots, \Sigma_p^{-1} \rrbracket \rangle. \quad (22)$$

We define the tensor differential of an inner product with respect to  $\Upsilon$  using the matrix differential  $\langle \partial \Upsilon, \mathcal{S} \rangle = \text{tr}(\partial \Upsilon_{(1)} \mathcal{S}'_{(1)})$ . Applying it to (22) yields

$$\partial \ell(\Upsilon) = \frac{1}{\sigma^2} \langle \partial \Upsilon, \llbracket \mathcal{S}; \Sigma_1^{-1}, \Sigma_2^{-1}, \dots, \Sigma_p^{-1} \rrbracket \rangle, \quad \text{where } \mathcal{S} = \sum_{i=1}^n \mathcal{Y}_i - \langle \sum_{i=1}^n \mathcal{X}_i | \mathcal{B} \rangle - n\Upsilon.$$

Now,  $\partial \ell(\Upsilon) = 0$  if  $\mathcal{S} = 0$ , and therefore (after profiling on  $\mathcal{B}$ ), the MLE of  $\Upsilon$  is

$$\hat{\Upsilon}(\mathcal{B}) = \frac{1}{n} \sum_{i=1}^n \mathcal{Y}_i - \langle \frac{1}{n} \sum_{i=1}^n \mathcal{X}_i | \mathcal{B} \rangle. \quad (23)$$

Setting  $\Upsilon$  in (22) to be  $\hat{\Upsilon}(\mathcal{B})$  in (23) yields the loglikelihood in (21) with centered responses and covariates, so we assume (20) has no intercept. We optimize (21) using a block-relaxation algorithm [35] that partitions the parameter space into multiple blocks and iteratively optimizes the parameter inside each block while keeping the parameters in the other blocks fixed at their current value. We discuss these blocks next.

2) *Estimation of  $\sigma^2$  under fixed  $\mathcal{B}, \Sigma_1, \Sigma_2, \dots, \Sigma_p$* : The first block optimizes (21) with respect to  $\sigma^2$  while holding all the other parameters fixed, and is obtained by differentiation to be

$$\hat{\sigma}^2 = \frac{1}{nm} \sum_{i=1}^n \langle \mathcal{Y}_i - \langle \mathcal{X}_i | \mathcal{B} \rangle, [\mathcal{Y}_i - \langle \mathcal{X}_i | \mathcal{B} \rangle; \Sigma_1^{-1}, \Sigma_2^{-1}, \dots, \Sigma_p^{-1}] \rangle. \quad (24)$$

Unlike  $\hat{\Upsilon}$  in (23), this is not a profile MLE because the blocks corresponding to the scale matrices  $\Sigma_k$  also depend on  $\sigma^2$ . The other blocks in the algorithm consist of obtaining the MLEs of  $\Sigma_1, \Sigma_2, \dots, \Sigma_p$  and the factors in the low-rank format of  $\mathcal{B}$ . Given  $\hat{\sigma}^2$ , the log-likelihood function value at the estimated parameters is

$$\ell = -\frac{n}{2} \left[ m + m \log(2\pi\hat{\sigma}^2) + \sum_{k=1}^p (m_{-k} \log |\hat{\Sigma}_k|) \right].$$

3) *Estimation of  $\mathcal{B}, \Sigma_1, \Sigma_2, \dots, \Sigma_p$  under fixed  $\sigma$* : We now estimate the next blocks of parameters  $\mathcal{B}, \Sigma_1, \Sigma_2, \dots, \Sigma_p$  under fixed  $\sigma = \hat{\sigma}$ . The estimates simplify differently according to the format of  $\mathcal{B}$  so are considered individually.

a) *Tucker format*:: Suppose that  $\mathcal{B}$  has Tucker format of rank  $(c_1, c_2, \dots, c_l, d_1, d_2, \dots, d_p)$ :

$$\mathcal{B}_{Tuck} = [\mathcal{V}; L_1, L_2, \dots, L_l, M_1, M_2, \dots, M_p], \quad M'_k \Sigma_k^{-1} M_k = I_{d_k}, \quad k = 1, \dots, p. \quad (25)$$

Then the number of parameters to be estimated goes down from the unconstrained  $\prod_{i=1}^l h_i \prod_{i=1}^p m_i$  to  $\prod_{i=1}^l c_i \prod_{i=1}^p d_i + \sum_{i=1}^l c_i h_i + \sum_{i=1}^p d_i m_i$ . The constraint  $M'_k \Sigma_k^{-1} M_k = I_{d_k}$  greatly simplifies estimation and inference. Using (25), we vectorize (20) as

$$\text{vec}(\mathcal{Y}_i) = \left( \bigotimes_{i=p}^1 M_i \right) \mathcal{V}'_{<l>} \text{vec}(\mathcal{W}_i) + \mathbf{e}_i, \quad \text{where } \mathcal{W}_i = [\mathcal{X}_i; L'_1, L'_2, \dots, L'_l], \quad (26)$$

and  $\mathbf{e}_i$ s are i.i.d  $\mathcal{N}_m(0, \sigma^2 \Sigma)$ . An alternative vectorized form of (20) writes

$$\text{vec}(\mathcal{Y}_i) = \mathcal{H}_{ik<2>}^{Tuck} \text{vec}(L_k) + \mathbf{e}_i, \quad k = 1, 2, \dots, l, \quad (27)$$

where  $\mathcal{H}_{ik<2>}^{Tuck}$  is the 2-canonical matricization of the tensor

$$\mathcal{H}_{ik}^{Tuck} = \mathcal{X}_i \times_{1, \dots, k-1, k+1, \dots, l} [\mathcal{V}; L_1, \dots, L_{k-1}, I_{h_k}, L_{k+1}, \dots, L_l, M_1, \dots, M_p]. \quad (28)$$

A tensor-network diagram of (28) is shown for the case where  $p = l = 3$  in Figure 5. The likelihood is optimized with respect to  $L_k, k = 1, 2, \dots, l$ , which forms its own block with the other parameters fixed. Then (27) is a multiple linear regression model and

$$\text{vec}(\widehat{L}_k) = \left( \sum_{i=1}^n \mathcal{H}_{ik<2>}^{Tuck} \Sigma^{-1} \mathcal{H}_{ik<2>}^{Tuck'} \right)^{-1} \left( \sum_{i=1}^n \mathcal{H}_{ik<2>}^{Tuck} \Sigma^{-1} \text{vec}(\mathcal{Y}_i) \right). \quad (29)$$

Now, we estimate  $(M_1, \Sigma_1), (M_2, \Sigma_2), \dots, (M_p, \Sigma_p)$  and  $\mathcal{V}$  under fixed  $L_1, L_2, \dots, L_p$  and  $\sigma^2$ . We first show that for fixed  $(M_1, \Sigma_1), (M_2, \Sigma_2), \dots, (M_p, \Sigma_p)$ ,  $\mathcal{V}$  can be profiled from the loglikelihood. Using (26), we get (21) to be

$$\ell(\mathcal{V}, M_1, \Sigma_1, M_2, \Sigma_2, \dots, M_p, \Sigma_p) = -\frac{n}{2} \log |\Sigma| - \frac{1}{2\sigma^2} \left\{ \text{tr}(Z' \Sigma^{-1} Z) \right\}, \quad (30)$$

where  $Z = Y - \left( \bigotimes_{k=p}^1 M_k \right) \mathcal{V}'_{<l>} W$  with  $Y = [\text{vec } \mathcal{Y}_1 \text{ vec } \mathcal{Y}_2 \dots \text{vec } \mathcal{Y}_n]$  and  $W = [\text{vec } \mathcal{W}_1 \text{ vec } \mathcal{W}_2 \dots \text{vec } \mathcal{W}_n]$ . Optimizing (30) with fixed  $(M_1, \Sigma_1), (M_2, \Sigma_2), \dots, (M_p, \Sigma_p)$  yields the profiled MLE

$$\hat{\mathcal{V}}_{<l>}(M_1, \Sigma_1, \dots, M_p, \Sigma_p) = W^{-'} Y' \left( \bigotimes_{k=p}^1 \Sigma_k^{-1} M_k \right), \quad (31)$$

where  $W^{-}$  is the right inverse of  $W$ . Therefore, given values of all blocks  $(M_k, \Sigma_k)$ , we obtain  $\hat{\mathcal{V}}$  by simply using them in (31). Now we consider each pair  $(M_k, \Sigma_k)$  as its own block, with loglikelihood obtained by replacing (31) in (30) and expressing it as

$$\ell(M_k, \Sigma_k) = -\frac{nm-k}{2} \log |\Sigma_k| - \frac{1}{2\sigma^2} \left\{ \text{tr}(Y' \Sigma^{-1} Y) - \|M'_k \Sigma_k^{-1} Q_k\|_2^2 \right\}, \quad (32)$$

where  $Q_k$  equals

$$[\mathcal{V}_T; M'_1 \Sigma_1^{-1}, M'_2 \Sigma_2^{-1}, \dots, M'_{k-1} \Sigma_{k-1}^{-1}, I_{m_k}, M'_{k+1} \Sigma_{k+1}^{-1}, M'_{k+2} \Sigma_{k+2}^{-1}, \dots, M'_p \Sigma_p^{-1}, W^- W]_{(k)} \quad (33)$$



and  $\mathcal{Y}_T \in \mathbb{R}^{m_1 \times m_2 \times \dots \times m_p \times n}$  is such that  $\mathcal{Y}_T(:, \dots, :, i) = \mathcal{Y}_i$  for  $i = 1, 2, \dots, n$ . From (32), the profile (on  $\Sigma_k$ ) MLE of  $M_k$  is obtained via generalized SVD of  $Q_k$  [36]:

$$\hat{M}_k(\Sigma_k) = \arg \max_{M_k: M_k' \Sigma_k^{-1} M_k = I_{d_k}} \|M_k' \Sigma_k^{-1} Q_k\|_2^2 = \Sigma_k^{1/2} U, \quad (34)$$

with the leading  $d_k$  left singular vectors of  $\Sigma_k^{-1/2} Q_k$  as the columns of  $U$ . We estimate  $\Sigma_k$  by inserting (34) into (32) and get

$$\ell(\Sigma_k) = -\frac{nm-k}{2} \log |\Sigma_k| - \frac{1}{2\sigma^2} \text{tr}(\Sigma_k^{-1} S_k), \quad S_k = \sum_{i=1}^n \mathcal{Y}_{i(k)} \Sigma_{-k}^{-1} \mathcal{Y}_{i(k)}' - Q_k Q_k'. \quad (35)$$

The MLE of  $\Sigma_k$  under the (Tucker format) constraint of (25) is

$$\hat{\Sigma}_k = \arg \max_{\Sigma_k: \Sigma_k[1,1]=1} \ell(\Sigma_k) = ADJUST(nm_k, \sigma^2, S_k), \quad (36)$$

where the *ADJUST* procedure is as introduced in [37] and that was shown to satisfy the Karush-Kuhn-Tucker (KKT) conditions. Without this constraint, the MLE is  $S_k/(nm-k\sigma^2)$ . We can impose parameterized structures on  $\Sigma_k$  by optimizing (35) numerically. For instance, when  $\Sigma_k$  is the covariance matrix of a stationary Gaussian process, the restriction  $\Sigma_k(1,1) = 1$  makes it the correlation matrix of the process. Based on our previous steps, the estimation of each  $\Sigma_k$  yields  $M_k$  using (34), and the estimation of all pairs  $(M_k, \Sigma_k)$  provides  $\mathcal{V}$  upon using (31). Algorithm 1 details the steps. Initialization and convergence of this algorithm are discussed in Section III-B4.

---

**Algorithm 1:** Block relaxation algorithm for Tensor-on-Tensor regression as in (16), where  $\mathcal{B}$  has the Tucker format  $\llbracket \mathcal{V}; L_1, L_2, \dots, L_l, M_1, M_2, \dots, M_p \rrbracket$ , and for  $k = 1, 2, \dots, p$ ,  $\Sigma_k[1,1] = 1$  and  $M_k' \Sigma_k^{-1} M_k = I_{d_k}$ .

---

**Input:** Initial values  $\hat{\sigma}^{2(0)}, \hat{\mathcal{V}}^{(0)}, \hat{L}_2^{(0)}, \hat{L}_3^{(0)}, \dots, \hat{L}_l^{(0)}, \hat{M}_1^{(0)}, \hat{\Sigma}_1^{(0)}, \hat{M}_2^{(0)}, \hat{\Sigma}_2^{(0)}, \dots, \hat{M}_p^{(0)}, \hat{\Sigma}_p^{(0)}$

- 1  $k = 0$
- 2 Center  $\mathcal{X}_i$  and  $\mathcal{Y}_i$  for  $i = 1, 2, \dots, n$  while storing the means  $\bar{\mathcal{X}}, \bar{\mathcal{Y}}$ .
- 3 **while** *convergence criteria is not met* **do**
- 4     **for**  $j = 1, 2, \dots, l$  **do**
- 5          $\hat{L}_j^{(k+1)}$  as per (29)
- 6     **end**
- 7     **for**  $j = 1, 2, \dots, p$  **do**
- 8          $(\hat{\Sigma}_j^{(k+1)}, \hat{M}_j^{(k+1)})$  as per (36) and (34)
- 9     **end**
- 10      $\hat{\mathcal{V}}^{(k+1)}$  as per (31)
- 11      $\hat{\sigma}^{2(k+1)}$  as per (24)
- 12      $k \leftarrow k + 1$
- 13 **end**
- 14  $\hat{\mathcal{Y}} = \bar{\mathcal{Y}} - \langle \bar{\mathcal{X}} | \llbracket \hat{\mathcal{V}}^{(k)}; \hat{L}_1^{(k)}, \hat{L}_2^{(k)}, \dots, \hat{L}_l^{(k)}, \hat{M}_1^{(k)}, \hat{M}_2^{(k)}, \dots, \hat{M}_p^{(k)} \rrbracket \rangle$

---

b) CP format:: We now optimize (21) when  $\mathcal{B}$  has CP format of rank  $r$ :

$$\mathcal{B}_{CP} = \llbracket \mathcal{X}; L_1, L_2, \dots, L_l, M_1, M_2, \dots, M_p \rrbracket. \quad (37)$$

The CP format is the most common tensor factorization and is preferred when the tensor modes are of similar sizes. Under this format and with  $\Sigma_k = I_{m_k}$  for  $k = 1, 2, \dots, p$ , (20) reduces to the framework of [38]. The CP format reduces the number of parameters in  $\mathcal{B}$  from  $\prod_{i=1}^p m_i \prod_{i=1}^l h_i$  to  $r(\sum_{i=1}^p m_i + \sum_{i=1}^l h_i)$ . Here also, we optimize (21) via a block-relaxation algorithm. The first  $p$  blocks corresponding to  $(M_1, \Sigma_1), (M_2, \Sigma_2), \dots, (M_p, \Sigma_p)$  can each be estimated in a MVMLR framework by applying Theorem II.2(3) on the  $k$ th mode matricized form of (20):

$$\mathcal{Y}_{i(k)} = M_k G_{ik}^{CP} + E_i, \quad E_i \stackrel{iid}{\sim} \mathcal{N}_{m_k, m_{-k}}(0, \sigma^2 \Sigma_k, \Sigma_{-k}), \quad k = 1, 2, \dots, p, \quad (38)$$

where  $G_{ik}^{CP} \equiv \mathcal{G}_{ik(k)}^{CP}$  is the  $k$ th mode matricization of

$$\mathcal{G}_{ik}^{CP} = \llbracket [\mathcal{X}_i; L'_1, \dots, L'_l] | \mathcal{I}_r^{p+l}; M_1, \dots, M_{k-1}, I_{m_k}, M_{k+1}, \dots, M_p \rrbracket.$$

In Section S2-A1, we further simplify  $G_{ik}^{CP}$  using the Khatri-Rao product ( $\odot$ ) [19], and in Figure 5, we provide a tensor-network diagram of  $\mathcal{G}_{ik}^{CP}$  for the case where  $p = l = 3$ . When all parameters other than  $(M_k, \Sigma_k)$  are held constant, (38) is the same as a MVMLR model and has loglikelihood

$$\ell(\Sigma_k, M_k) = \frac{nm-k}{2} \log |\Sigma_k^{-1}| - \frac{1}{2\sigma^2} \text{tr}(\Sigma_k^{-1} S_k), \quad (39)$$

with  $S_k = \sum_{i=1}^n Z_{ik} \Sigma_{-k}^{-1} Z'_{ik}$ , where  $Z_{ik} = \mathcal{Y}_{i(k)} - M_k G_{ik}^{CP}$ . Then the MLEs are

$$\hat{M}_k = \sum_{i=1}^n \mathcal{Y}_{i(k)} \Sigma_{-k}^{-1} G_{ik}^{CP'} \left[ \sum_{i=1}^n G_{ik}^{CP} \Sigma_{-k}^{-1} G_{ik}^{CP'} \right]^{-1}, \quad \hat{\Sigma}_k(M_k) = ADJUST(nm_{-k}, \sigma^2, S_k). \quad (40)$$

The matrix  $\sum_{i=1}^n G_{ik}^{CP} \Sigma_{-k}^{-1} G_{ik}^{CP'}$  in (40) is further simplified in Section S2-A1. As with the Tucker format, we estimate  $\Sigma_k$  by directly optimizing (39). The other  $l$  blocks in the block-relaxation algorithm correspond to  $L_1, L_2, \dots, L_l$  and are each multiple linear regression models obtained by vectorizing (20) as:

$$\text{vec}(\mathcal{Y}_i) = H_{ik}^{CP} \text{vec}(L_k) + e_i, \quad e_i \stackrel{iid}{\sim} \mathcal{N}_m(0, \sigma^2 \Sigma), \quad k = 1, 2, \dots, l, \quad (41)$$

where  $H_{ik}^{CP} = \mathcal{H}_{ik<2>}^{CP}$  and  $\mathcal{H}_{ik}^{CP}$  is identical to the  $\mathcal{H}_{ik}^{Tuck}$  of (28), but for the fact that  $\mathcal{V}$  is the diagonal tensor  $\mathcal{I}_r^{p+l}$ . A tensor-network diagram of  $\mathcal{H}_{ik}^{CP}$  is provided in figure 5 for the case where  $p = l = 3$ . For  $k = 1, 2, \dots, l$ , holding all parameters except  $L_k$  constant makes (41) a MLR model with the MLE of  $L_k$  obtained as

$$\text{vec}(\hat{L}_k) = \left( \sum_{i=1}^n H_{ik}^{CP} \Sigma^{-1} H_{ik}^{CP'} \right)^{-1} \left( \sum_{i=1}^n H_{ik}^{CP} \Sigma^{-1} \text{vec}(\mathcal{Y}_i) \right). \quad (42)$$

The matrix  $\sum_{i=1}^n H_{ik}^{CP} \Sigma^{-1} H_{ik}^{CP'}$  in equation (42) is further simplified in Section S2-A1. As summarized in Figure 5, the tensors  $\mathcal{H}_{ik}^{CP}$  and  $\mathcal{G}_{ik}^{CP}$  play a critical role in the practical estimation of  $M_k$  and  $L_k$  through (38) and (41), permitting the use of standard MVMLR and MLR estimation methods. From (8), we deduce that the  $j$ th columns of all the factor matrices in the CP decomposition (37) are identifiable up to a constant. To deal with this, we constrain these columns to have unit norm. The MLEs of our parameters are obtained using block-relaxation algorithm, as outlined in Algorithm 2.

---

**Algorithm 2:** Block-relaxation algorithm for Tensor-on-Tensor regression (16), with  $\mathcal{B}$  of CP format  $[\hat{\mathbf{X}}; L_1, L_2, \dots, L_l, M_1, M_2, \dots, M_p]$ . The CP factor matrices are all constrained to have unit column norm and  $\Sigma_k[1, 1] = 1$  for  $k = 1, 2, \dots, p$ .

---

**Input:** Initial values  $\hat{\sigma}^{2(0)}, \hat{L}_2^{(0)}, \hat{L}_3^{(0)}, \dots, \hat{L}_l^{(0)}, \hat{M}_1^{(0)}, \hat{M}_2^{(0)}, \dots, \hat{M}_p^{(0)}$

- 1  $k = 0$
- 2 Center  $\mathcal{X}_i$  and  $\mathcal{Y}_i$  for  $i = 1, 2, \dots, n$  while saving the means  $\bar{\mathcal{X}}, \bar{\mathcal{Y}}$ .
- 3 **while** convergence criteria is not met **do**
- 4     **for**  $j = 1, 2, \dots, l$  **do**
- 5          $\hat{L}_j^{(k+1)}$  as per (42) and normalize its columns
- 6     **end**
- 7     **for**  $j = 1, 2, \dots, p - 1$  **do**
- 8          $(\hat{M}_k^{(k+1)}, \hat{\Sigma}_k^{(k+1)})$  as per (40) and normalize the columns of  $\hat{M}_k^{(k+1)}$
- 9     **end**
- 10      $(\hat{M}_p^{(k+1)}, \hat{\Sigma}_p^{(k+1)})$  as per (40)
- 11      $\hat{\sigma}^{2(k+1)}$  as per (24)
- 12     Normalize the columns of  $\hat{M}_p^{(k+1)}$  while setting  $\hat{\mathbf{X}}^{(k+1)}$  to those norms
- 13      $k = k + 1$
- 14 **end**
- 15  $\hat{\mathbf{Y}} = \bar{\mathcal{Y}} - \langle \bar{\mathcal{X}} | [\hat{\mathbf{X}}^{(k)}; \hat{L}_1^{(k)}, \hat{L}_2^{(k)}, \dots, \hat{L}_l^{(k)}, \hat{M}_1^{(k)}, \hat{M}_2^{(k)}, \dots, \hat{M}_p^{(k)}] \rangle$

---

c) OP format:: For an OP-formatted  $\mathcal{B}$ , that is

$$\mathcal{B}_{OP} = \circ[M_1, M_2, \dots, M_p], \quad (43)$$

we apply Theorem II.1(2) to express (20) as

$$\mathcal{Y}_i = [\mathcal{X}_i; M_1, \dots, M_p] + \mathcal{E}_i, \quad \text{with } \mathcal{E}_i \stackrel{iid}{\sim} \mathcal{N}_{m_1, \dots, m_p}(0, \sigma^2 \Sigma_1, \Sigma_2, \dots, \Sigma_p), \quad i = 1, \dots, n. \quad (44)$$

To estimate the parameters in (44), we apply the  $k$ th mode matricization on both sides

$$\mathcal{Y}_{i(k)} = M_k G_{ik}^{OP} + E_i, \quad E_i \stackrel{iid}{\sim} \mathcal{N}_{m_k, m_{-k}}(0, \sigma^2 \Sigma_k, \Sigma_{-k}), \quad k = 1, 2, \dots, p, \quad (45)$$

where  $G_{ik}^{OP} = \mathcal{X}_{i(k)} \left( \bigotimes_{j=p, j \neq k}^1 M_j' \right)$ . Given the similarities between (38) and (45), the MLEs of the factor matrices are as in (42) but with  $G_{ik}^{OP}$  instead of  $G_{ik}^{CP}$ . The optimization procedure is similar to Algorithm 2, with the difference again that  $M_1, M_2, \dots, M_{p-1}$  are normalized to have unit Frobenius norm. We conclude by noting that (44) is the multilinear tensor regression setup of [39], and for  $p = 2$  is the matrix-variate regression framework of [40] and [41]. So the OP format generalizes and frames existing methodology to the tensor-on-tensor regression framework.

d) TR format:: Let  $\mathcal{B}$  have TR format (11) of TR rank  $(s_1, s_2, \dots, s_l, g_1, g_2, \dots, g_p)$ . Then

$$\mathcal{B}_{TR} = \text{tr}(\mathcal{L}_1 \times^1 \mathcal{L}_2 \times^1 \dots \times^1 \mathcal{L}_l \times^1 \mathcal{M}_1 \times^1 \mathcal{M}_2 \times^1 \dots \times^1 \mathcal{M}_p). \quad (46)$$

This means that  $\mathcal{L}_j$  and  $\mathcal{M}_k$  are third order tensor of sizes  $(s_{j-1} \times h_j \times s_j)$  and  $(g_{k-1} \times m_k \times g_k)$  respectively, for all  $j = 1, 2, \dots, l$  and  $k = 1, 2, \dots, p$ , and where  $g_0 = s_l$  and  $s_0 = g_p$ . The TR format reduces the number of unconstrained parameters in  $\mathcal{B}$  from  $\prod_{i=1}^l h_i \prod_{i=1}^p m_i$  to  $\sum_{j=1}^l s_{j-1} h_j s_j + \sum_{k=1}^p g_{k-1} m_k g_k$ . Unlike the CP format, the TR format does not impose a global restriction on the sizes of the factors, making it convenient to use when the tensor modes are of very different sizes. To estimate parameters, we apply the  $k$ -th mode matricization and vectorization to both sides of (16), yielding

$$\mathcal{Y}_{i(k)} = \mathcal{M}_{(2)}^{(k)} G_{ik}^{TR} + E_i, \text{ where } E_i \stackrel{iid}{\sim} \mathcal{N}_{m_k, m-k}(0, \sigma^2 \Sigma_k, \Sigma_{-k}), \quad k = 1, 2, \dots, p \quad (47)$$

and

$$\text{vec}(\mathcal{Y}_i) = H_{ik}^{TR} \text{vec}(\mathcal{L}^{(k)}) + e_i, \text{ where } e_i \stackrel{iid}{\sim} \mathcal{N}_{m_1 \times \dots \times m_p}(0, \sigma^2 \Sigma) \quad k = 1, 2, \dots, l, \quad (48)$$

where  $G_{ik}^{TR}$  and  $H_{ik}^{TR}$  are matrices as defined in Section S2-A2. Figure 5 uses tensor-network diagrams to display tensor-variate versions of  $H_{ik}^{TR}$  and  $G_{ik}^{TR}$  for when  $p = l = 3$ . Because of the similarities of (38) and (41) with (47) and (48), the ML estimators of our parameters mirror the CP format case but by replacing  $(H_{ik}^{CP}, G_{ik}^{CP})$  with  $(H_{ik}^{TR}, G_{ik}^{TR})$ . In this case, estimating  $(M_k, \text{vec}(L_k))$  corresponds to estimating  $(\mathcal{M}_{k(2)}, \text{vec}(\mathcal{L}_k))$ . The optimization procedure is similar to Algorithm 2, with the difference that here each factor tensor other than  $\mathcal{M}_p$ , is scaled to have unit Frobenius norm.

4) *Initialization and convergence*: For local optimality, we need the two conditions that the log-likelihood  $\ell$  is jointly continuous and that the set  $\{\theta : \ell(\theta) \geq \ell(\theta^{(0)})\}$ , for a set of initial values  $\theta^{(0)}$ , is compact [35]. These conditions are satisfied because of the TVN distributional assumption on our errors, as long as the initial values satisfy the constraints on the parameters. We initialized  $\Sigma_k = I_{m_k}$  and the tensor factor entries in  $\mathcal{B}$  with draws from the  $\mathcal{U}(0, 1)$  distribution. With the Tucker format,  $M_k$  has the constraint  $M_k' \Sigma_k^{-1} M_k = I_{d_k}$  for  $k = 1, 2, \dots, p$ , so we used  $\Sigma_k^{1/2} U$  as its initializer, with  $U$  having the left singular vectors of a random matrix of the same order as  $M_k$ . Our preliminary studies showed improved initial values for the tensor factors in  $\mathcal{B}$  by running the algorithm to lax convergence while setting  $\sigma^2 = 1$  and the scale matrices  $(\Sigma_1, \Sigma_2, \dots, \Sigma_p)$  to identity matrices, and fitting the MLE algorithm of [25] to the residuals of this fit to obtain the initial value of  $\sigma^2$  as  $\prod_{k=1}^p \Sigma_k(1, 1)$ , and setting the initial value of  $\Sigma_k$  as  $\Sigma_k / \Sigma_k(1, 1)$ . We adopt this strategy in our experiments in this paper.

Our algorithms are declared to converge when we have negligible changes in the loglikelihood, as simplified in (III-B2). A different criteria is the difference in norm  $\|\mathcal{B}\| + \|\sigma^2 \Sigma\|$ , where  $\|\sigma^2 \Sigma\| = \sigma \prod_{k=1}^p \|\Sigma_k\|$  and  $\|\mathcal{B}\|$  simplifies as per format:

- for  $\mathcal{B}_{Tucker}$  as in (25),  $\|\mathcal{B}_{Tucker}\| = \|\llbracket \mathcal{V}; L_1^q, L_2^q, \dots, L_l^q, M_1^q, M_2^q, \dots, M_p^q \rrbracket\|$ , where  $A^q$  is the Q matrix from the LQ decomposition of  $A$  [26].
- for  $\mathcal{B}_{CP}$  as in (37),  $\|\mathcal{B}_{CP}\|^2 = \sum_{k=1}^R \sum_{l=1}^R \{ \text{diag}(\lambda) [*_{i=1}^l (L_i' L_i)] * [*_{i=1}^p (M_i' M_i)] \} (k, l)$ , where “\*” is the Hadamard, or entry-wise product [26].
- for  $\mathcal{B}_{OP}$  as in (43),  $\|\mathcal{B}_{OP}\| = \prod_{i=1}^p \|M_i\|$ .

a) *Overview*:: We conclude this section by summarizing in Figure 5 our estimation methods for  $\mathcal{B}$  in for different formats, with the use of block-relaxation algorithms. We see that in many cases, an algorithmic block can be made to correspond to a linear model by choosing  $\mathcal{G}_{ik}$  or  $\mathcal{H}_{ik}$  appropriately. Then, fitting a tensor-response linear model involves sequentially fitting smaller-dimensional linear models (one for each tensor factor) until convergence. This intuition behind the estimation of  $\mathcal{B}$  is not restricted only to the Tucker, CP, OP and TR formats used in this paper, but can help guide estimation algorithms for other formats.

### C. Asymptotic sampling distributions of the estimators

We now derive the asymptotic distributions of our model-estimated parameters, specifically, the linear component (Section III-C1) and the covariance component (Section III-C2). For the remainder of this paper, we define  $h \doteq \prod_{i=1}^l h_i$ ,  $M \doteq \bigotimes_{i=p}^1 M_i$  and  $L \doteq \bigotimes_{i=l}^1 L_i$ .

1) *Distribution of the linear components*: Regardless of the format of  $\mathcal{B}$ , the estimated factors have exact known distributions because they are obtained as part of a linear model with normal errors. We first assume that (20) holds without an intercept.

**Theorem III.1.** *Let (20) hold with  $\mathcal{B} \equiv \mathcal{B}_{Tucker}$  of Tucker format as in (25). Then*

$$\text{vec}(\hat{\mathcal{B}}_{Tucker}) \xrightarrow{d} \mathcal{N}_{mh} \left( \text{vec}(\mathcal{B}_{Tucker}), \sigma^2 (MM') \otimes (P_L (X X')^{-1} P_L) \right) \quad \text{as } n \rightarrow \infty, \quad (49)$$

where  $\hat{\mathcal{B}}_{Tucker} = \llbracket \hat{\mathcal{V}}; \hat{L}_1, \hat{L}_2, \dots, \hat{L}_l, \hat{M}_1, \hat{M}_2, \dots, \hat{M}_p \rrbracket$ ,  $X = [\text{vec}(\mathcal{X}_1) \dots \text{vec}(\mathcal{X}_n)]$  and  $P_L = \bigotimes_{i=l}^1 P_i$  with  $P_i = L_i (L_i' L_i)^{-1} L_i'$ .

*Proof.* See Section S2-B. □

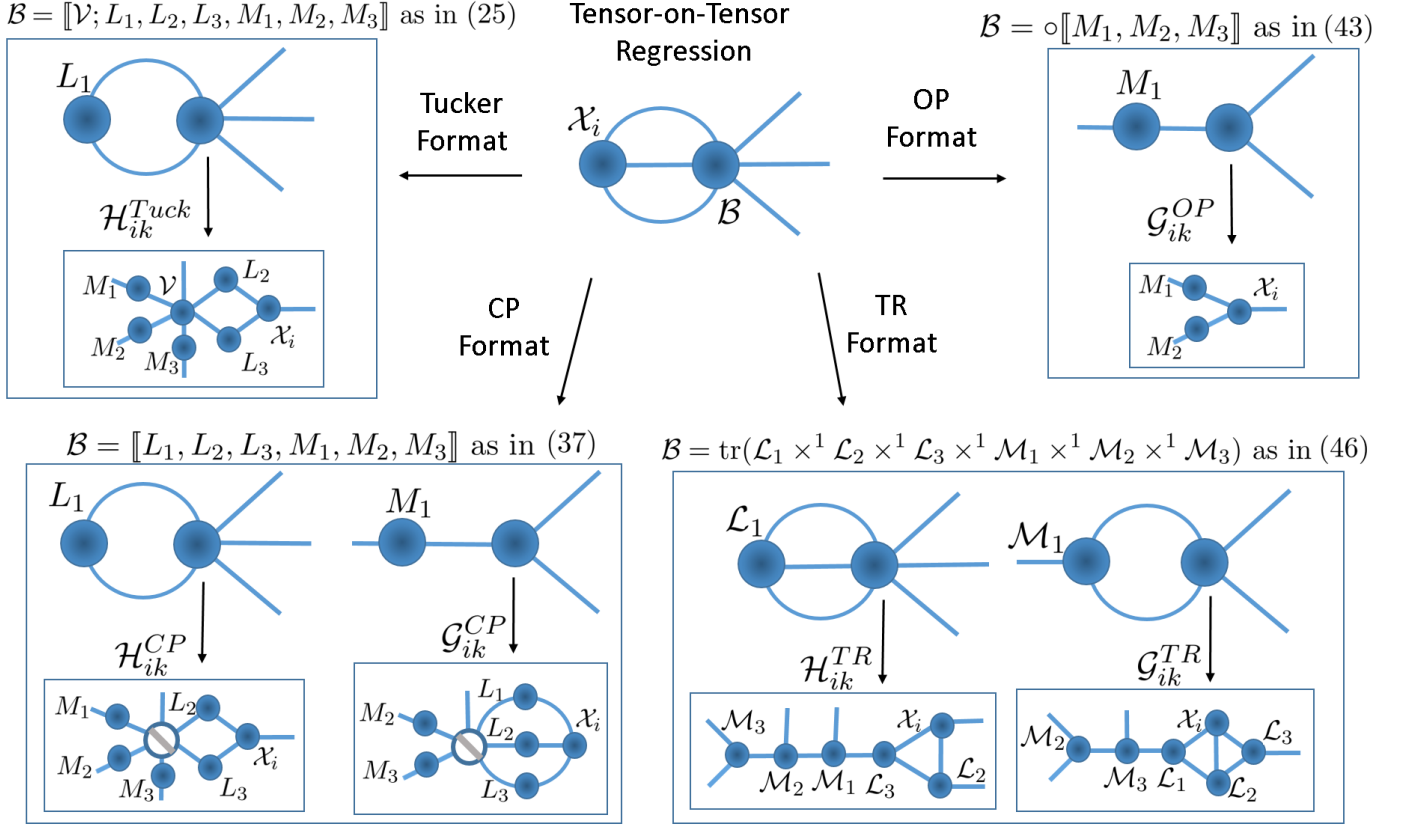


Fig. 5: Equivalent tensor-network diagrams for  $(\mathcal{X}_i, \mathcal{B})$  when  $p = l = 3$ , which can be expressed in multiple ways depending on the tensor factor to be estimated and the type of low-rank on  $\mathcal{B}$  (which are illustrated in Figure 4). By choosing the tensors  $\mathcal{G}_{ik}$  and  $\mathcal{H}_{ik}$ , the tensors  $M_1$  and  $M_1$  can be estimated using multivariate multiple linear regression, and the tensors  $L_1$  and  $\mathcal{L}_1$  can be estimated using multiple linear regression, respectively. In these cases, matricized versions of  $\mathcal{G}_{ik}$  and  $\mathcal{H}_{ik}$  are part of the design matrix.

The distribution in (49) is TVN when  $XX'$  has a Kronecker structure: examples include factorial designs and B-splines [42]. Here we present one such case.

**Corollary III.1.** When  $\hat{\mathcal{B}}_{Tucker}$  is used to estimate a balanced TANOVA as in (20) with  $q$  experimental units for each combination of factors, then

$$\hat{\mathcal{B}}_{Tucker} \xrightarrow{d} \mathcal{N}_{h_1, \dots, h_l, m_1, \dots, m_p}(\mathcal{B}, \frac{\sigma^2}{q} P_1, P_2, \dots, P_l, M_1 M_1', M_2 M_2', \dots, M_p M_p') \quad \text{as } n \rightarrow \infty. \quad (50)$$

*Proof.* Here  $XX' = qI_h$  and so the variance-covariance matrix in (49) is  $(\sigma^2/q)(MM') \otimes (\bigotimes_{i=1}^l P_i)$ , which is Kronecker-separable. The result follows from Definition II.2.  $\square$

The CP format case is similar to Theorem III.1, but has a different asymptotic variance:

**Theorem III.2.** Consider (20) with  $\mathcal{B} \equiv \mathcal{B}_{CP}$  as in (37) and the ML estimators

$$\begin{aligned} \hat{\mathcal{B}}_{CP} &= [\hat{L}_1, \hat{L}_2, \dots, \hat{L}_l, \hat{M}_1, \hat{M}_2, \dots, \hat{M}_p] \\ \hat{\Theta}_{CP} &= [\text{vec}(\hat{L}_1)' \text{vec}(\hat{L}_2)' \dots \text{vec}(\hat{L}_l)' \text{vec}(\hat{M}_1)' \text{vec}(\hat{M}_2)' \dots \text{vec}(\hat{M}_p)']'. \end{aligned}$$

$$\text{Then, } \text{vec}(\hat{\mathcal{B}}_{CP}) \xrightarrow{d} \mathcal{N}_{m \times h} \left( \text{vec}(\mathcal{B}_{CP}), J_{CP} R_{CP} (\mathbf{I}_n \otimes \Sigma) R_{CP}' J_{CP}' \right) \quad \text{as } n \rightarrow \infty.$$

Here the Jacobian matrix  $J_{CP} = \frac{\partial}{\partial \hat{\Theta}_{CP}} \text{vec}(\hat{\mathcal{B}}_{CP})$  is a block matrix with blocks as per Lemma S2.1(a), and  $R_{CP} = [A_1' A_2' \dots A_l' B_1' B_2' \dots B_p']'$ , where

$$A_k = [S_{1k}^{-1} H_{1k}^{CP} \Sigma^{-1} \dots S_{lk}^{-1} H_{lk}^{CP} \Sigma^{-1}], \quad S_{1k} = \sum_{i=1}^n H_{ik}^{CP} \Sigma^{-1} H_{ik}^{CP'}, \quad k = 1, 2, \dots, l,$$

$$B_k = [S_{2k}^{-1} G_{1k}^{CP} \Sigma_{-k}^{-1} \dots S_{2k}^{-1} G_{nk}^{CP} \Sigma_{-k}^{-1}] \otimes I_{m_k}, \quad S_{2k} = \sum_{i=1}^n G_{ik}^{CP} \Sigma_{-k}^{-1} G_{ik}^{CP'}, \quad k = 1, 2, \dots, p.$$

Recall also that  $S_{1k}$  and  $S_{2k}$  are simplified in Section S2-A1.

*Proof.* See Section S2-C. □

The sampling distributions of  $\mathcal{B}$  under the OP or TR formats are similar to the CP case, and are in Section S2-E.

**Theorem III.3.** For a model with intercept, as in (16), Theorems III.1 and III.2 also hold after centering the covariates.

*Proof.* See Section S2-F. □

2) *Distribution of the scale components:* Our final result is on the distribution of the estimated scale matrices  $\hat{\Sigma}_1, \hat{\Sigma}_2, \dots, \hat{\Sigma}_p$ . We obtain the Fisher information matrix and show that it is singular.

**Theorem III.4.** Let  $\theta_\Sigma = [(\text{vech } \Sigma_1)', \text{vech } \Sigma_2)', \dots, (\text{vech } \Sigma_p)']'$ , where  $\Sigma_1, \Sigma_2, \dots, \Sigma_p$  are scale matrices with no restrictions on their proportionality, and  $\text{vech}$  is the half-vectorization mapping, as discussed further in Section S1. Then

- 1) The joint linear components  $\begin{bmatrix} \text{vec}(\hat{\mathbf{Y}}) \\ \text{vec}(\hat{\mathbf{B}}) \end{bmatrix}$  and  $\hat{\theta}_\Sigma$  are asymptotically independent regardless of the format of  $\hat{\mathbf{B}}$ .
- 2) The Fisher information with respect to  $\theta_\Sigma$ , denoted as  $\mathbb{I}_\Sigma$ , is a block matrix with  $k$ th block diagonal matrices ( $k = 1, 2, \dots, p$ ) given by

$$\mathbb{E} \left( - \frac{\partial^2 \ell(\Sigma_k)}{\partial(\text{vech } \Sigma_k) \partial(\text{vech } \Sigma_k)'} \right) = \frac{nm-k}{2} D'_{m_k} (\Sigma_k^{-1} \otimes \Sigma_k^{-1}) D_{m_k} \quad (51)$$

and  $(k, l)$ th block matrices for  $k \neq l$ ,  $k, l = 1, 2, \dots, p$ , given as

$$\mathbb{E} \left( - \frac{\partial^2 \ell(\Sigma_k, \Sigma_l)}{\partial(\text{vech } \Sigma_k) \partial(\text{vech } \Sigma_l)'} \right) = \frac{nm-kl}{2} D'_{m_k} (\text{vec}(\Sigma_k^{-1}) \text{vec}(\Sigma_l^{-1})') D_{m_l}, \quad (52)$$

where  $D_{m_k}$  is the duplication matrix of Section S1 and  $m_{-kl} = \prod_{i=1, i \neq k, i \neq l}^p m_i$ .

- 3) The Fisher information  $\mathbb{I}_\Sigma$  is singular.

*Proof.* See Section S2-G. □

a) *Comment::* Our results on the asymptotic distribution of the scale components are not unique to our regression methodology but also generally hold for the TVN distribution.

#### IV. EXPERIMENTAL EVALUATIONS

In this section, we study estimation performance of the scale parameters and the low-rank linear component  $\mathcal{B}$  using simulation experiments on different tensor-on-tensor regression models. In Section IV-A we study the consistency of our estimators, while in Section IV-B we evaluate the amounts of recovery that different low-rank formats have of  $\mathcal{B}$ , and the impact of noise on discrimination in a TANOVA framework.

##### A. Matrix-on-matrix regression

We simulated observations from the matrix-on-matrix regression model

$$Y_{ijk} = \langle X_{ij} | \mathcal{B} \rangle + E_{ijk}, \quad E_{ijk} \stackrel{iid}{\sim} \mathcal{N}_{6,7}(0, \sigma^2 \Sigma_1, \Sigma_2), \quad i = 1, 2, 3, 4, \quad j = 1, 2, 3, 4, 5, \quad (53)$$

where  $X_{ij}$  is a  $4 \times 5$  matrix with 1 at the  $(i, j)$ th position and zeroes everywhere else. We set  $\sigma^2 = 1$  and simulated  $\Sigma_1$  and  $\Sigma_2$  independently from Wishart distributions, that is,  $\Sigma_1 \sim \mathcal{W}_6(6, I_6)$  and  $\Sigma_2 \sim \mathcal{W}_7(7, I_7)$ , before scaling each by their  $(1, 1)$ th element. We generated data from four matrix-on-matrix regression models, one for each model with  $\mathcal{B}$  of Tucker, CP, TR and OP formats, and fit appropriate models to the data, using the ML procedures described in Section III. To study consistency properties of our estimators, we used  $k = 1, 4, 7, 10$  and  $13$ , meaning that our sample sizes ranged over  $n \in \{20, 80, 140, 200, 260\}$ . A constrained  $\mathcal{B}$  in this experiment would have  $4 \times 5 \times 6 \times 7 = 840$  entries. For the OP format, our  $\mathcal{B}$  is chosen to have only 59 unconstrained parameters, while for the CP case, we set  $\mathcal{B}$  to have rank 2 and only 45 unconstrained parameters. The number of free parameters was only 60 when  $\mathcal{B}$  was set to be of Tucker format with rank  $(2, 2, 2, 2)$  and 70 when  $\mathcal{B}$  had the TR format of rank  $(2, 2, 2, 2)$ . Thus, our lower-rank simulation framework for  $\mathcal{B}$  was chosen to have at least 91% fewer free elements as the full-structured  $\mathcal{B}$ . We simulated data from (53) using  $\mathcal{B}$ ,  $\sigma^2$  and  $\Sigma_1$  and  $\Sigma_2$  and estimated the parameters using our method for each replication. Figure 6 displays the Frobenius norm of the difference between the true and estimated parameters, and shows that with increasing sample size,  $(\hat{\mathcal{B}}, \hat{\sigma}^2, \hat{\Sigma}_1, \hat{\Sigma}_2)$  approach the true parameters  $(\mathcal{B}, \sigma^2, \Sigma_1, \Sigma_2)$ , demonstrating consistency of the estimators.

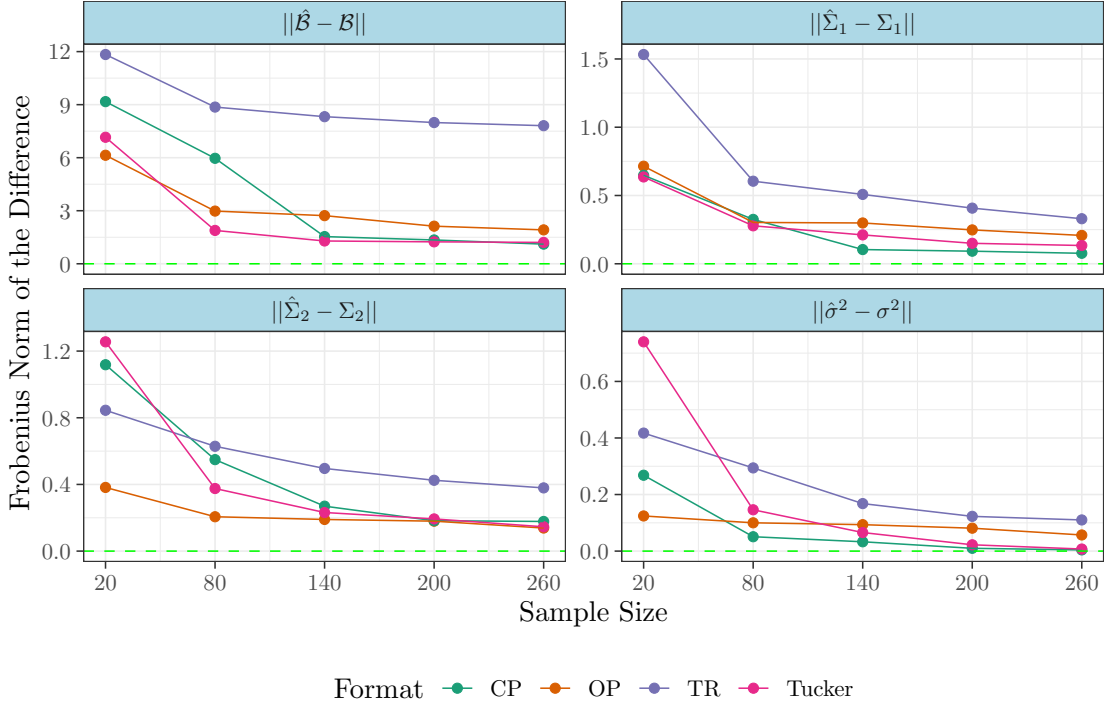


Fig. 6: Performance of the four models presented in Section IV-A, each corresponding to a different format on  $\mathcal{B}$ . Each of the four plots correspond to the Frobenius norm of the difference between the estimated and the true population parameter, against the sample size. We observe that in all cases, an increase in sample size leads to more accurate estimates.

### B. TANOVA(2,2) model

We simulated 600 total observations from

$$Y_{ijk} = \Upsilon_{ij} + E_{ijk}, \quad E_{ijk} \stackrel{iid}{\sim} \mathcal{N}_{87,106}(0, \sigma^2 \Sigma_1, \Sigma_2), \quad i = 1, 2, 3, 4 \quad j = 1, 2, 3, \quad (54)$$

where  $\Upsilon_{ij}$  corresponds to the pixel-wise logit transformation of the  $j$ th additive color (Red, Green, Blue) of the  $i$ th Andean camelid (Guanaco, Llama, Vicuña, Alpaca) images of Figure 7. The scale matrices  $\Sigma_1$  and  $\Sigma_2$  were set to AR(1) correlation matrices with coefficients 0.1 and  $-0.1$  respectively, and  $\sigma^2 = 1$ . Without any restrictions, we have  $3 \times 4 \times 87 \times 106 = 110,664$  parameters in the twelve different means  $\Upsilon_{ij}$ . To estimate all these parameters simultaneously we fit the four TANOVA(2,2) models

$$Y_{ijk} = \langle X_{ij} | \mathcal{B} \rangle + E_{ijk} \sim \mathcal{N}_{87,106}(0, \omega^2 \Omega_1, \Omega_2), \quad i = 1, 2, 3, 4 \quad j = 1, 2, 3, \quad (55)$$

that correspond to the TR, Tucker, CP and OP formats on  $\mathcal{B}$ . The scale matrices  $\Omega_1$  and  $\Omega_2$  were both estimated as AR(1) correlation matrices and the ranks of the formats were chosen so that the number of free parameters in  $\mathcal{B}$  are comparable. The TR format with rank (3,3,5,3) resulted in 2958 parameters in  $\mathcal{B}$ , the Tucker format with rank (4,4,9,9) had 3061 parameters, the CP format with rank 15 yielded 3001 parameters and the OP format reduced the number of parameters to 666. In all cases there was a dimension reduction in  $\mathcal{B}$  of over 97%. For each format, the estimated tensor  $\hat{\mathcal{B}}$  is of size  $4 \times 3 \times 87 \times 106$ , and it corresponds to the estimated color images of the four Andean camelids. The estimated images are presented in Figure 7, where we can observe different amounts of success in recovering the underlying camelid image. The OP case gives images with the least-resolved features, with the reduced number of parameters for  $\mathcal{B}$  inadequate for recovery. Unlike OP, the other formats can adjust for the quantum of reduction in parameters through their ranks. We illustrate this aspect by fitting (55) with  $\mathcal{B}$  having a Tucker format with rank (3, 4, 66, 68), which was chosen by Bayesian information criterion (BIC) [43], [44] out of 81 different candidate ranks. Figure 7 (last column) points to very good recovery of  $\mathcal{B}$  with unappreciable visual differences between the estimated and true images.

The TANOVA(2,2) formulation of (54) enables us to test the set of hypothesis

$$H_0 : \mathcal{P}_1 = \mathcal{P}_2 = \mathcal{P}_3 = \mathcal{P}_4, \text{ vs. } H_a : \mathcal{P}_i \neq \mathcal{P}_{i^*}, \text{ for some } i \neq i^* \in \{1, 2, 3, 4\} \quad (56)$$

where  $\mathcal{P}_i$  is the third-order tensor of size  $3 \times 87 \times 106$  that contains the RGB slices of the  $i$ th Andean camelid image. Under the null hypothesis, the four Andean camelids' images are indistinguishable from each other while the alternative hypothesis specifies at least one of them to be different from the other images. The usual Wilks'  $\Lambda$  statistic [45] is

$$\Lambda = |\hat{\Sigma}_R| / |\hat{\Sigma}_T|, \quad (57)$$





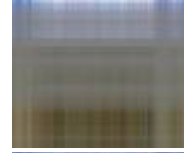




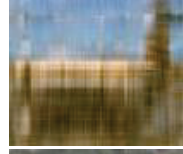
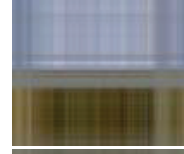





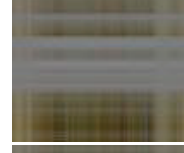
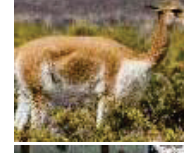


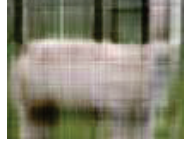


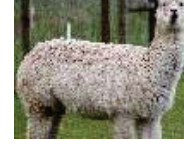
	True Image	TR	Tucker	CP	OP	Optimal Tucker
Guanaco						
Llama						
Vicuña						
Alpaca						
BIC	—	$1.6959 \times 10^7$	$1.6978 \times 10^7$	$1.6925 \times 10^7$	$1.7722 \times 10^7$	$1.6148 \times 10^7$
Rank	—	(3,3,5,3)	(4,4,9,9)	15	—	(4,3,66,68)
Parameters	—	2961	3064	3003	669	66834

Fig. 7: Results of fitting four different TANOVA(2,2) models on data simulated from (54). The four models correspond to four distinct low-rank formats (TR, Tucker, CP and OP) and the two factors to the type of andean camelid (Guanaco, Llama, Vicuña, Alpaca) and the type of additive color RGB (red, green, blue). The Guanaco, Llama and Alpaca images are from Wikipedia and the Vicuña image is from Encyclopædia Britannica. In most cases the true image gets restored. The resolution of the TR, Tucker and the CP format can be adjusted with the ranks, and the resolution of the OP is low because of the small number of parameters involved. The last column, corresponding to a Tucker fit of rank (4, 3, 66, 68) that has the best BIC from among 81 candidate models of different Tucker ranks, essentially recovers the true images.

where  $\Sigma_R$  is the sample covariance matrix of the residuals after fitting (55)

$$\hat{\Sigma}_R = \sum_{i=1}^4 \sum_{j=1}^3 \sum_{k=1}^{50} (\text{vec}(Y_{ijk} - \langle X_{ij} | \hat{\mathcal{B}} \rangle)) (\text{vec}(Y_{ijk} - \langle X_{ij} | \hat{\mathcal{B}} \rangle))',$$

with appropriate  $\mathcal{B}$  and  $\hat{\mathcal{B}}$  is its estimate. The matrix  $\hat{\Sigma}_T$  is the sample covariance matrix of the simpler model's residuals, which finds a common mean across all camelids, and is formally written as

$$\Sigma_T = \sum_{i=1}^4 \sum_{j=1}^3 \sum_{k=1}^{50} (\text{vec}(Y_{ijk} - \langle X_{ij}^* | \hat{\mathcal{B}}^* \rangle)) (\text{vec}(Y_{ijk} - \langle X_{ij}^* | \hat{\mathcal{B}}^* \rangle))',$$

where  $X_{ij}^*$  is a matrix of the same size as  $X_{ij}$  but contains zeroes everywhere except in its  $i$ th row, where it contains only ones. The tensor  $\hat{\mathcal{B}}^*$  is the low-rank estimator of  $\mathcal{B}^*$ , both of size  $3 \times 4 \times 87 \times 106$  and contains 4 copies of the camelids' image means, each of size  $3 \times 87 \times 106$ . The tensor  $\hat{\mathcal{B}}^*$  is obtained from fitting (55) with  $X_{ij}^*$  instead of  $X_{ij}$  for all  $i = 1, 2, 3, 4$  and  $j = 1, 2, 3$ . We assume that  $\hat{\mathcal{B}}$  and  $\hat{\mathcal{B}}^*$  have the same low-rank format and rank, and so the hypotheses in (56) are stated to have the same constraints of format and rank. The matrices  $\Sigma_R$  and  $\Sigma_T$  are non-negative definite of size  $9222 \times 9222$  and rank 600, so each determinant in (57) is the product of its 600 singular eigenvalues. We illustrate the role of  $\sigma$  and the low-rank OP, TR, CP or Tucker format in distinguishing the four camelids, as measured by the Wilks'  $\Lambda$  test statistic, in Figure 8, for  $\sigma^2 = 5, 25, 100, 225, 400$ . The value of  $\Lambda$  increases with  $\sigma^2$ , meaning that larger variances decrease the power of our test. Further, the CP, TR and Tucker formats have lower-valued (more significant) test statistics than the OP format. This finding illustrates the limits of the OP format relative to the others, because of its lower flexibility in meeting the level of recovery of  $\mathcal{B}$ . Nevertheless, this example illustrates consistency of the estimation and discrimination, as per Wilks'  $\Lambda$ , for all four formats.



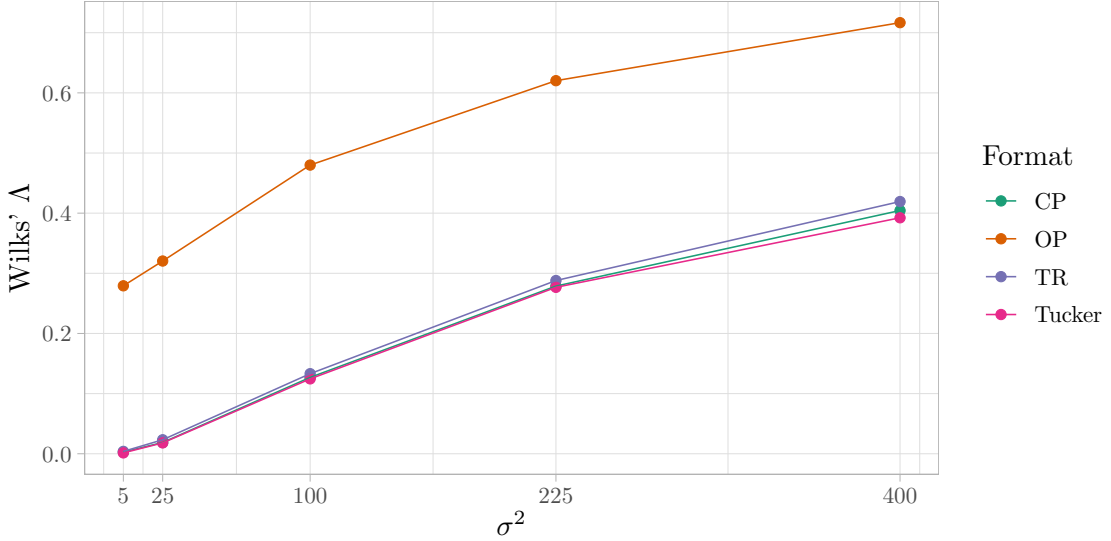


Fig. 8: Wilks'  $\Lambda$  statistics that correspond to the set of hypothesis in equation (56) for four low-rank formats of OP, CP, TR and Tucker, and five values of scalar variance  $\sigma^2$  in the x-axis. We observe that large variabilities lead to larger test statistics, and therefore weaker evidence against the null hypothesis. We also observe that CP, TR and Tucker lead to more significant statistics when compared to the OP. Overall, all values of  $\Lambda$  are small, meaning that the groups are significantly different.

## V. REAL DATA APPLICATIONS

Having evaluated performance of our reduced-rank tensor-on-tensor regression methodology in simulation experiments, we now apply it to the datasets introduced in Section I-A.

### A. A $TANOVA(1,5)$ model for cerebral activity in suicide-at-risk subjects

In Section I-A1 we described a TANOVA model involving 30 fMRI volumes, each corresponding to one of 10 words connoting death, positive or negative affects, of voxel-wise percent changes in activation, from a baseline, for each of 17 subjects. For the  $j$ th subject we have a fifth-order tensor  $\mathcal{Y}_j$  of order  $3 \times 10 \times 43 \times 56 \times 20$ , where the first two modes correspond to the three kinds of word stimulus and the individual words, and the other modes correspond to the dimensions of the image volume. The  $j$ th subject is one of type  $i$  (1 for attempter and 2 for ideator) with status as in  $\mathbf{x}_j$  that is a 2D unit vector with 1 at position  $i$ . We model these responses and covariates as

$$\mathcal{Y}_j = \langle \mathbf{x}_j | \mathcal{B} \rangle + \mathcal{E}_j, \quad \mathcal{E}_j \stackrel{iid}{\sim} \mathcal{N}_{3,10,43,56,20}(0, \sigma^2 \Sigma_1, \Sigma_2, \Sigma_3, \Sigma_4, \Sigma_5), \quad (58)$$

where  $j = 1, 2, \dots, 17$ . We let  $\mathcal{B}$  have a sixth-order tensor structure of Tucker format with rank  $(2, 3, 6, 15, 20, 7)$  chosen, using BIC, out of a total of 256 candidate ranks

$$\mathcal{B} = \llbracket \mathcal{V}; L_1, M_1, M_2, M_3, M_4, M_5 \rrbracket, \quad M'_k \Sigma_k^{-1} M_k = I_{d_k}, \quad k = 1, 2, 3, 4, 5. \quad (59)$$

The 77,578 parameters in the Tucker-formatted  $\mathcal{B}$  to be estimated represent a substantial (over 97.3%) reduction over that of an unconstrained  $\mathcal{B}$ , which is of size  $2 \times 3 \times 10 \times 43 \times 56 \times 20$  and contains over 2,889,600 free parameters. (Our use of a Tucker format conveniently exploits its nicer distributional properties to make inference easier.) We set  $\Sigma_1$  (specifying relationships between word types) to be unconstrained,  $\Sigma_2$  (covariances between words within a certain type) to have an equicorrelation structure and  $\Sigma_3, \Sigma_4, \Sigma_5$  with AR(1) correlation structures to capture spatial context in the 3D image volume.

Our primary interest here is to find regions of significant interactions between word type and subject suicide attempter/ideator status to determine markers for suicide risk assessment and intervention. From Theorem III.1 and Definition II.2, we have, as  $n \rightarrow \infty$ ,

$$\hat{\mathcal{B}} \xrightarrow{d} \mathcal{N}_{2,3,10,43,56,20}(\mathcal{B}, \sigma^2 P_1 (X X')^{-1} P_1, M_1 M'_1, M_2 M'_2, M_3 M'_3, M_4 M'_4, M_5 M'_5), \quad (60)$$

where  $X X'$  is a diagonal matrix with two non-zero entries (9, 8). Using (60), we estimate the 3-level interaction as  $\hat{\mathcal{B}}_* = \hat{\mathcal{B}} \times_1 \mathbf{c}'_1 \times_2 C_2 \times_3 \mathbf{c}'_3$ , where  $\mathbf{c}_1 = (1, -1)'$  is a contrast vector that finds differences between suicide attempter/ideation status,  $\mathbf{c}_3 = (1, 1, \dots, 1)'/10$  a contrast vector that averages the 10 words of each word type, and

$$C_2 = \begin{bmatrix} 1 & 0 & -1 \\ 1 & -1 & 0 \\ 0 & -1 & 1 \end{bmatrix} \quad (61)$$



is a contrast matrix for differences across word type. The tensor  $\hat{B}_*$  contains all the interactions; for instance, the first row of  $C_2$  finds differences between the first and third word types, so the first level interaction  $\hat{B}_*(1, :, :, :)$

$$\frac{1}{10} \sum_{k=1}^{10} \left( \hat{B}(1, 1, k, :, :, :) - \hat{B}(1, 3, k, :, :, :) - \hat{B}(2, 1, k, :, :, :) + \hat{B}(2, 3, k, :, :, :) \right),$$

identifies regions of significant differences in how death- and negative-connoted words affect suicide ideators and attempters. Similarly, the second row of  $C_2$  finds differences between the first two word types, so the second level interaction  $\hat{B}_*(2, :, :, :)$  is

$$\frac{1}{10} \sum_{k=1}^{10} \left( \hat{B}(1, 1, k, :, :, :) - \hat{B}(1, 2, k, :, :, :) - \hat{B}(2, 1, k, :, :, :) + \hat{B}(2, 2, k, :, :, :) \right),$$

and its significant regions correspond to locations with a significant difference in how the contrast between death-related and positive-connoting words affect suicide ideators and attempters. Finally, the third row of  $C_2$  finds differences between the first and third word types and so the third-level interaction  $\hat{B}_*(3, :, :, :)$  is

$$\frac{1}{10} \sum_{k=1}^{10} \left( \hat{B}(1, 3, k, :, :, :) - \hat{B}(1, 2, k, :, :, :) - \hat{B}(2, 3, k, :, :, :) + \hat{B}(2, 2, k, :, :, :) \right),$$

and its significant regions correspond to locations with a significant difference in how the contrast between negative- and positive-connoting words affect suicide ideators and attempters. From (60), (61) and Lemma II.2, the asymptotic distribution of  $\hat{B}_*$  is

$$\hat{B}_* \xrightarrow{d} \mathcal{N}_{3,20,43,56}(\mathcal{B}_*, \tau^2 C_2 M_1 M_1' C_2', M_3 M_3', M_4 M_4', M_5 M_5'), \quad (62)$$

where  $\tau^2 = \sigma^2 \times (c_1' P_1 (X X')^{-1} P_1 c_1) \times (c_3' M_2 M_2' c_3)$  and  $\mathcal{B}_* = \mathcal{B} \times_1 c_1' \times_2 C_2 \times_3 c_3'$ . Using (62), we marginally standardize  $\hat{B}_*$  using the Tucker product and Lemma II.2 to obtain

$$\hat{\mathcal{Z}}_* = [\hat{B}_*; d_2(\tau^2 C_2 M_1 M_1' C_2'), d_2(M_3 M_3'), d_2(M_4 M_4'), d_2(M_5 M_5')], \quad (63)$$

where  $d_2(A)$  is a diagonal matrix of the inverse square roots of the diagonal entries of  $A$ . Then  $\hat{\mathcal{Z}}_*(i, \cdot, \cdot, \cdot)$  has the TVN distribution, with correlation matrices as scale parameters. For the  $i$ th level interaction, consider the set of hypotheses at the  $(k, l, m)$ th voxel

$$H_o : \mathcal{B}_*(i, k, l, m) = 0 \quad \text{vs} \quad H_a : \mathcal{B}_*(i, k, l, m) \neq 0.$$

Under the null hypothesis of no  $i$ th interaction effect at the  $(k, l, m)$ th voxel, and from (62) and (63), the marginal distribution of  $\hat{\mathcal{Z}}_*(i, k, l, m)$  is asymptotically  $N(0, 1)$ .

Figure 9 displays 3D maps of the brain with significant values of  $\hat{\mathcal{Z}}_*$  overlaid for each of the three pairs of interactions. Significant voxels were decided using cluster-thresholding [46] at the 5% level of significance, with clusters of at least 12 contiguous (under a second-order neighborhood specification) and minimum cluster size determined by the Analysis for Neuroimaging (AFNI) software [47], [48]. There are many methods [49]–[55] for significance detection in fMRI studies but we use cluster thresholding here as an illustration and also because it is the most popular method. We now briefly discuss the results.

Figure 9(a) identifies significant interactions between death- and negative-connoting words on the one hand and suicide attempters vis-a-vis ideators on the other. All significant interactions are positive and dominated by the precuneus and the orbital frontal cortex. The precuneus is associated with depression and rumination [56]–[58], while the orbital frontal cortex is associated with the influence that emotions and feelings have on decision-making [59], as well as with suicide attempters' reactions to extraneous stimulus [60]. Both regions are also associated with the Default Mode Network (DMN) that plays a role in representing emotions [61]. These results indicate more differential rumination and emotions (between attempters and ideators) caused by death-related words, as compared to negative-connoting words. These findings are reinforced by the significance detected in the occipital lobe, the premotor cortex (PMC) and the superior parietal cortical regions that are related to working memory and depression [62]–[64]. Figure 9(b) displays significant interactions between the positive and death-related words and suicide attempters and ideators. The precuneus is more pronounced here relative to Figure 9(a), indicating that death-related words are more salient than both negative- and positive-implying words among attempters vis-a-vis ideators. This observation is reinforced with the detected significance in the dorsal and ventral visual medial prefrontal cortex, the mammillary bodies, and the posterior cingulate cortex (PCC) that are all involved in processing emotional information [65], [66]. The PCC is also involved in memory, emotion, and decision-making [67], [68] and is connected to the temporal-parietal junction [69] which is involved with emotions and perception [70], [71]. High  $\hat{\mathcal{Z}}_*$  values in the ventral and dorsal visual cortices are commensurate with their association with working memory tasks [72]. Also, the low values of  $\hat{\mathcal{Z}}_*$  in the temporal parietal junction point to needed additional processing of death-related versus positive-connoting words among attempters relative to ideators. Figure 9(c) shows significant interactions between negative and positive-emoting words and suicide attempters and ideators. The low values in the left and right temporal-parietal junctions and the PMC indicate that words conveying negative

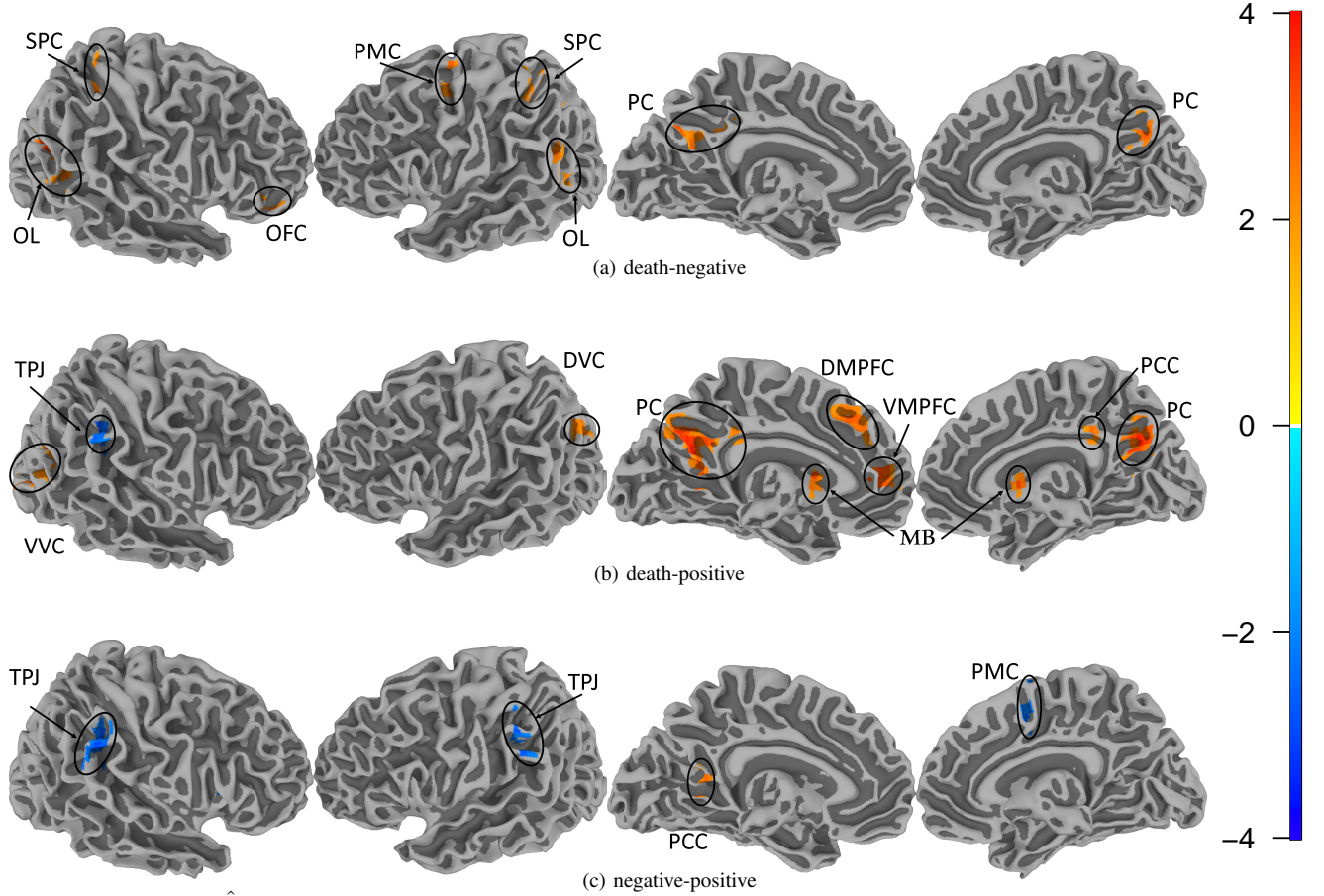


Fig. 9: The test statistic  $\hat{Z}_*$  of the interaction between subject's attempter/ideator status and (a) death-negative, (b) death-positive and (c) negative-positive words at voxels identified significant by cluster-thresholding at the 5% level. These voxels are in the precuneus (PC), temporal-parietal junction (TPJ), orbital frontal cortex (OFC), premotor cortex (PMC), superior parietal cortex (SPC), ventral visual cortex (VVC), dorsal visual cortex (DVC), dorsal medial frontal cortex (DMPFC), ventral medial prefrontal cortex (VMPFC), mamillary bodies (MB), posterior cingulate cortex (PCC) and occipital lobe (OL).

thoughts don't need as much processing as do positive-connoting words among attempters relative to ideators. The significance in the PCC reported in both Figures 9(b) and (c) supports our hypothesis that death-related words are more salient than negative or positive words in differentiating attempters from ideators. In summary, the two groups of subjects have positive- and negative-connoting words result in neurally similar significant brain regions when compared to death-related words, which show further significance in areas associated with the processing of emotional feelings and planning. Further analysis of our results is needed because our conclusions here are on an experiment with only 9 attempters and 8 ideators, but are interpretable, providing some confidence in the practical reductions afforded by TANOVA when coupled with the use of the Tucker-formatted  $\mathcal{B}$  for this application.

#### B. A TANOVA(3,3) model for the LFW face database

We return to the LFW faces database of Section I-A2 that is a compendium of over 13,000 face images from online sources. The ethnic origin and age-group assignments of these images are from the classifier of [15] that provided values of attributes that are positive for its presence and negative otherwise, along with magnitudes that describe the degree to which the attribute is present or absent (these magnitudes cannot be compared between different attributes). Since these attributes are for all age groups and ethnic origins, we have ambiguous classification for a large majority of the images. We removed ambiguities in age group and ethnic origin by selecting images where (for each factor) the maximum attribute is positive and the other attributes are negative. The genders were as per [14]'s manual assignments of each image. We considered images only of male or female genders, and discarded those that have no or both gender assignments. These two filters reduced the number of images to 5,472. Although these 5,472 images had non-ambiguous attributes, they were very imbalanced, as 37% of them corresponded to only one of the  $2 \times 3 \times 4 = 24$  factor-combinations (senior males of European ethnicity). While our TANOVA model can handle imbalance, it can provide inaccurate information for the underrepresented factor-combinations. Therefore, we

randomly selected at most 33 images for each factor combination, reducing the sample size from 5,472 to 605. (This dataset was also used by [38] in the context of tensor-on-tensor regression with the CP format, but with the goal of classification, leading to a vector-response of attribute values and tensor-valued covariates of color images. In contrast, our interest is to distinguish characteristics of different attributes, leading to a TANOVA(3,3) model with color images as the response and the non-ambiguous factors of gender, ethnic origin and gender as covariates.) Our model is as per (20) and specifically

$$\mathcal{Y}_{ijkl} = \langle \mathcal{X}_{ijk} | \mathcal{B} \rangle + \mathcal{E}_{ijkl}, \quad \mathcal{E}_{ijkl} \sim \mathcal{N}_{151,111,3}(0, \sigma^2 \Sigma_1, \Sigma_2, \Sigma_3),$$

$$i = 1, 2, \quad j = 1, 2, 3, \quad k = 1, 2, 3, 4, \quad l = 1, 2, \dots, n_{ijk},$$

where the  $(i, j, k, l)$ th response  $\mathcal{Y}_{ijkl}$  is the color image of size  $151 \times 111 \times 3$  that corresponds to the  $l$ th person with the  $i$ th gender,  $j$ th ethnic origin and  $k$ th age group. We used the inner  $151 \times 111 \times 3$  portion of the original  $250 \times 250 \times 3$  voxels where the third dimension corresponds to the color intensities in RGB format, and the logit transformation was applied to every value to match the statespace of the normal distribution. Here  $\mathcal{X}_{ijk} = e_i^2 \circ e_j^3 \circ e_k^4$  is the tensor-valued covariate for a TANOVA(3,3) model with  $(h_1, h_2, h_3) = (2, 3, 4)$ , as described in Section III-A2, encoding the genders  $\times$  ethnic-origin  $\times$  age-group attributes of  $\mathcal{Y}_{ijkl}$ .

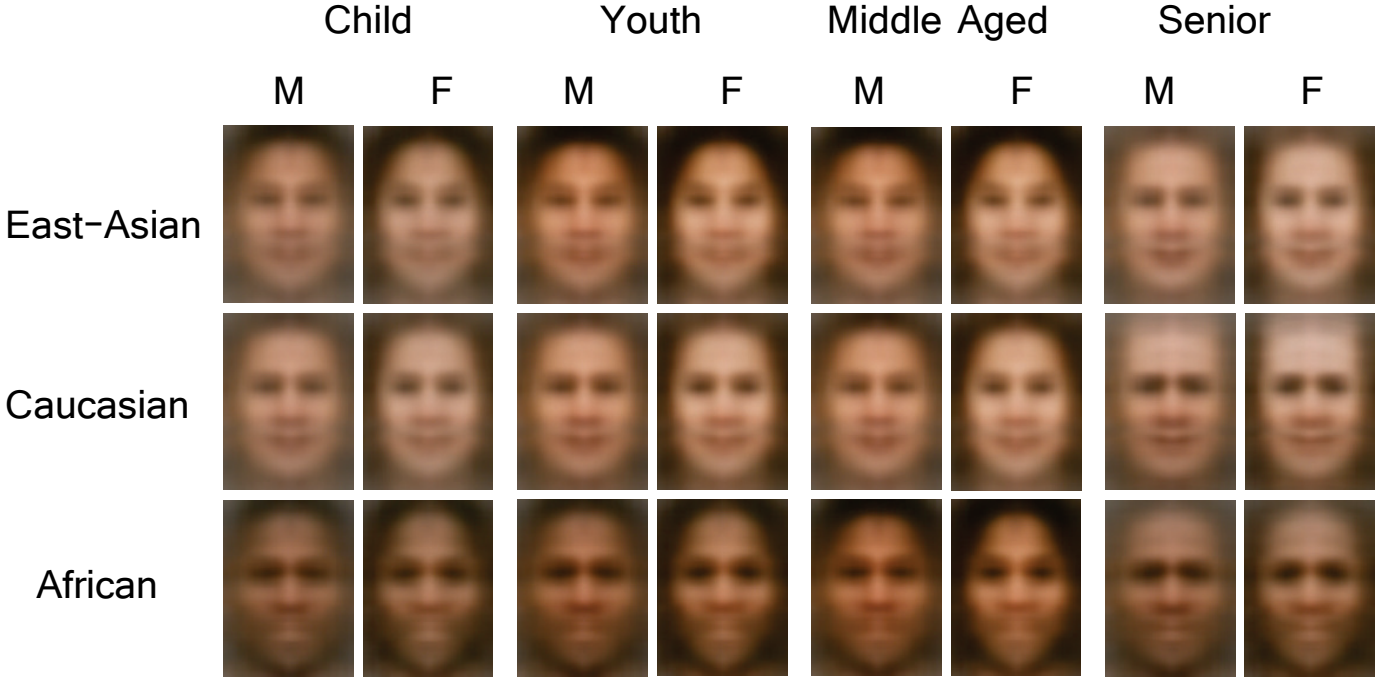


Fig. 10: Different slices of the resulting factorized tensor  $\mathcal{B}$  that results from fitting a TANOVA(3,3) model on the LFW dataset using the TT format. The results are compressed mean images across genders (male, female), ethnic origin (East-Asian, Caucasian, African) and age groups (child, youth, middle aged and senior) from 605 central LFW images. We can observe that the TT format preserved vital information regarding the factor-combination of age group, gender and ethnic-origin.

The corresponding TANOVA parameter  $\mathcal{B}$  is of size  $2 \times 3 \times 4 \times 151 \times 111 \times 3$  and contains all the group means. We constrained  $\mathcal{B}$  to a tensor train (TT) format of TR rank  $(1, 3, 3, 4, 10, 3)$ , which was chosen using BIC out of a total of 64 candidate ranks. (The TT format also bested, in terms of the BIC, the Tucker, CP and OP formats.) The number of parameters involved in  $\mathcal{B}$  is 6,393 due to the TT restriction, which is a reduction in the number of unconstrained parameters of around 99% from the unconstrained  $\mathcal{B}$  that has more than 1.2 million parameters. Figure 10 displays the estimated  $\hat{\mathcal{B}}$ , from where we observe that the TT format preserved visual information regarding ethnic origin, gender, and age-group.

## VI. DISCUSSION

In this paper, we have provided a multivariate regression and analysis of variance framework that exploits the tensor-valued structure of the explanatory and response variables using four different low-rank formats on the regression coefficient and a Kronecker separable structure on the covariance matrix. These structures are imposed for practical reasons, as the number of parameters involved in the classical multivariate regression model grows exponentially with the tensor dimensions. However, different ranks on the regression coefficient result in different models, which can be compared between each other using criteria such as BIC. Further, we provided algorithms for ML estimation and evaluated them via simulation experiments. We studied the asymptotic properties of our estimators and applied our methodology to identify brain regions associated with suicide

attempt status and words connoting death or negative or positive thoughts. We also used our methods to distinguish facial characteristics in the LFW dataset.

There are several other avenues for further investigation. First, we can perform additional dimension reduction by adding an  $L_1$  penalty on the likelihood optimization. Also, the number of parameters in the intercept can be potentially large when the tensor response is high-dimensional, which motivates specifying a low-rank structure on the intercept term. Similarly, the independent identically distribution assumption on the errors is not feasible when external factors group data-points into units that are similar to one another. For these cases, a mixed-effects model is more appropriate. Further, it would be worth investigating if we can generalize the Kronecker separability structure of the errors or the normality assumption to incorporate more general distributional forms. These are some issues that may benefit from further attention and that we leave for future work.

#### ACKNOWLEDGMENTS

The authors are very grateful to B. Klinedinst and A. Willette of the Program of Neuroscience and the Department of Food Sciences and Human Nutrition for help with the interpretation of Figure 9. This research was supported in part by the National Institute of Justice (NIJ) under Grants No. 2015-DN-BX-K056 and 2018-R2-CX-0034. The research of the second author was also supported in part by the National Institute of Biomedical Imaging and Bioengineering (NIBIB) of the National Institutes of Health (NIH) under Grant R21EB016212, and the United States Department of Agriculture (USDA) National Institute of Food and Agriculture (NIFA) Hatch project IOW03617. The content of this paper is however solely the responsibility of the authors and does not represent the official views of the NIJ, the NIBIB, the NIH, the NIFA or the USDA.

#### SUPPLEMENTARY MATERIALS

##### S1. SUPPLEMENT TO SECTION II

###### A. Some Matrix Algebra Properties

In this section we provide identities and detail notation used in the main paper, in preparation for the proof of Lemma II.1 and Theorem II.1. While the  $\text{vec}(\cdot)$  operator stacks the columns of a matrix into a vector, the commutation matrix  $K_{k,l} \in \mathbb{R}^{kl \times kl}$  matches the elements of  $\text{vec}(A)$  and  $\text{vec}(A')$ ,

$$\text{vec}(A') = K_{k,l} \text{vec}(A), \quad A \in \mathbb{R}^{k \times l}. \quad (\text{S1})$$

The commutation matrix plays a critical role in tensor algebra, as it allows us to reshape tensors inside their vectorization. If  $A$  is a symmetric  $n \times n$  matrix, then  $\text{vec}(A)$  has  $n^2$  elements of which  $n(n-1)/2$  are repetitions, while the half-vectorization  $\text{vech}(A)$  contains the  $n(n+1)/2$  unique elements of  $A$ , since it does not take into account the elements above the diagonal. The duplication matrix  $D_n$  maps the elements of  $\text{vec}(A)$  and  $\text{vech}(A)$  as  $D_n \text{vech}(A) = \text{vec}(A)$ , and is a full-column rank matrix of size  $n^2 \times (n(n+1)/2)$ . The following is from [73]:

**Properties S1.1.** Let  $A_1 \in \mathbb{R}^{m \times n}$  and  $A_2 \in \mathbb{R}^{p \times q}$  and  $K_{\cdot,\cdot}$  be a commutation matrix. Then

a.  $K_{\cdot,\cdot}$  is orthogonal and flipping the arguments results in its transpose. That is,

$$K'_{m,n} = K_{m,n}^{-1} = K_{n,m}.$$

b.  $K_{\cdot,\cdot}$  can be used to change the order of the Kronecker product. That is,

$$K_{p,m}(A_1 \otimes A_2)K_{n,q} = A_2 \otimes A_1.$$

c.  $K_{\cdot,\cdot}$  can be used to split the Kronecker product inside the vectorization. That is,

$$\text{vec}(A_1 \otimes A_2) = R_{A_1} \text{vec}(A_2), \quad R_{A_1} = (I_n \otimes K_{q,m})(\text{vec } A_1 \otimes I_q).$$

The Kronecker product ( $\otimes$ ) between  $A$  and  $B$  results in the following block matrix:

$$A \otimes B = \begin{bmatrix} A(1,1)B & \dots & A(1,m)B \\ \vdots & \ddots & \vdots \\ A(n,1)B & \dots & A(n,m)B \end{bmatrix}. \quad (\text{S2})$$

The following properties follow recursively from the two-matrix cases in [74].

**Properties S1.2.** Let  $A_1, A_2, \dots, A_p$  be matrices of any size and  $\Sigma_1, \Sigma_2, \dots, \Sigma_p$  be positive definite matrices of any size. Then

- $\left| \bigotimes_{i=p}^1 \Sigma_i \right| = \prod_{i=1}^p |\Sigma_i|^{m_{-i}}, \quad m_{-i} = \prod_{j=1, j \neq i}^p \text{rank}(\Sigma_j).$
- $\left( \bigotimes_{i=p}^1 \Sigma_i \right)^{-1} = \left( \bigotimes_{i=p}^1 \Sigma_i^{-1} \right), \quad \left( \bigotimes_{i=p}^1 A_i \right)' = \left( \bigotimes_{i=p}^1 A_i' \right).$

c.  $\bigotimes_{i=p}^1 A_i = \left( \bigotimes_{i=p}^{l+1} A_i \right) \otimes \left( \bigotimes_{i=l}^1 A_i \right), \quad l = 2, \dots, p-2.$

d.  $\left( \bigotimes_{i=p}^1 A_i \right) \left( \bigotimes_{i=p}^1 B_i \right) = \bigotimes_{i=p}^1 (A_i B_i), \quad \text{where } A_i \text{ has as many columns as the rows of } B_i.$

### B. Some Tensor Algebra Properties

The vectorization,  $k$ th-mode matricization and the  $k$ th canonical matricization of a  $p$ -th order tensor  $\mathcal{X}$  of size  $m_1 \times m_2 \times \dots \times m_p$  as defined in Table I and Equation (4) are

$$\text{vec}(\mathcal{X}) = \sum_{i_1=1}^{m_1} \dots \sum_{i_p=1}^{m_p} \mathcal{X}_{(i_1 \dots i_p)} \left( \bigotimes_{q=p}^1 e_{i_q}^{m_q} \right), \quad (\text{S3})$$

$$\mathcal{X}_{(k)} = \sum_{i_1=1}^{m_1} \dots \sum_{i_p=1}^{m_p} \mathcal{X}(i_1 \dots i_p) e_{i_k}^{m_k} \left( \bigotimes_{\substack{q=p \\ q \neq k}}^1 e_{i_q}^{m_q} \right)', \quad (\text{S4})$$

and

$$\mathcal{X}_{<k>} = \sum_{i_1=1}^{m_1} \dots \sum_{i_n=1}^{m_p} \mathcal{X}(i_1 \dots i_p) \left( \bigotimes_{a=k}^1 e_{i_q}^{m_q} \right) \left( \bigotimes_{q=p}^{k+1} e_{i_q}^{m_q} \right)', \quad (\text{S5})$$

respectively. To illustrate these reshapings, consider the third-order tensor  $\mathcal{X} \in \mathbb{R}^{3 \times 4 \times 2}$  illustrated in Figure S1 and that was

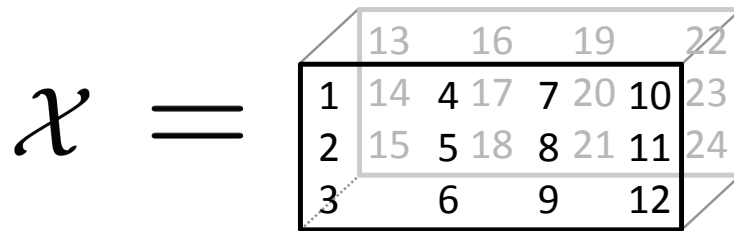


Fig. S1: A third order tensor  $\mathcal{X} \in \mathbb{R}^{3 \times 4 \times 2}$  with elements 1 through 24.

also used in [19]. The  $k$ th-mode matricizations are

$$\mathcal{X}_{(1)} = \begin{bmatrix} 1 & 4 & 7 & 10 & 13 & 16 & 19 & 22 \\ 2 & 5 & 8 & 11 & 14 & 17 & 20 & 23 \\ 3 & 6 & 9 & 12 & 15 & 18 & 21 & 24 \end{bmatrix}, \quad \mathcal{X}_{(2)} = \begin{bmatrix} 1 & 2 & 3 & 13 & 14 & 15 \\ 4 & 5 & 6 & 16 & 17 & 18 \\ 7 & 8 & 9 & 19 & 20 & 21 \\ 10 & 11 & 12 & 22 & 23 & 24 \end{bmatrix},$$

$$\mathcal{X}_{(3)} = \begin{bmatrix} 1 & 2 & 3 & 4 & 5 & 6 & 7 & 8 & 9 & 10 & 11 & 12 \\ 13 & 14 & 15 & 16 & 17 & 18 & 19 & 20 & 21 & 22 & 23 & 24 \end{bmatrix},$$

and the  $k$  canonical matricizations are

$$\mathcal{X}_{\langle 1 \rangle} = \mathcal{X}_{(1)}, \quad \mathcal{X}_{\langle 2 \rangle} = \mathcal{X}'_{(3)}, \quad \mathcal{X}_{\langle 3 \rangle} = \text{vec}(\mathcal{X}) = [1 \quad 2 \quad \dots \quad 24]'$$

The last-mode with first-mode contraction, denoted as  $\times^1$  and defined in Table II and Equation (5), is used to define the TR format in equation (11). One special case of this contraction is the matrix product between  $X$  and  $Y$ , which contracts the columns of  $X$  with the rows of  $Y$ , and can be expressed as  $X \times^1 Y$ . In Figure S2 we further illustrate this contraction, for the  $\mathcal{X}$  of Figure S1.

We can reshape tensors by manipulating the vector outer product ( $\circ$ ) applied to unit basis vectors, as in Equation (2). If  $\{e_k^{m_k}\}_{k=1}^p$  are unit basis vectors, then  $\bigotimes_{k=p}^1 e_k^{m_k}$  is also so, and so

$$\left(\bigotimes_{k=n}^1 e_k^{m_k}\right)' \left(\bigotimes_{k=n}^1 e_k^{m_k}\right) = \bigotimes_{k=n}^1 (e_k^{m_k'} e_k^{m_k}) = 1. \quad (\text{S6})$$

Equation (S6) is helpful in simplifying matrix products between matricized tensors.

$$\mathcal{X} \times^1 \begin{bmatrix} 1 & 2 \\ 1 & 2 \end{bmatrix} = \begin{array}{|c|c|c|c|} \hline & 28 & 40 & 52 & 64 \\ \hline 14 & 32 & 20 & 44 & 26 & 56 & 32 & 68 \\ \hline 16 & 36 & 22 & 48 & 28 & 60 & 34 & 72 \\ \hline 18 & & 24 & & 30 & & 36 & \\ \hline \end{array}$$

Fig. S2: The third order tensor that results from applying the last-mode with first-mode contraction between  $\mathcal{X}$  and  $Y$ , where  $\mathcal{X}$  is as in Figure S1.

### C. Proof of Lemma II.1

*Proof.*

(a) We have

$$\begin{aligned} \mathcal{X}'_{<p-1>} &= \sum_{i_1=1}^{m_1} \dots \sum_{i_p=1}^{m_p} \mathcal{X}(i_1, i_2, \dots, i_p) \left( \left( \bigotimes_{q=p-1}^1 e_{i_q}^{m_q} \right) (e_{i_p}^{m_p})' \right)' \\ &= \sum_{i_1=1}^{m_1} \dots \sum_{i_p=1}^{m_p} \mathcal{X}(i_1, i_2, \dots, i_p) \left( (e_{i_p}^{m_p}) \left( \bigotimes_{q=p-1}^1 e_{i_q}^{m_q} \right)' \right) = \mathcal{X}_{(p)}. \end{aligned}$$

(b) For any  $l = 1, 2, \dots, p$ , we have

$$\begin{aligned} \text{vec}(\mathcal{X}_{<l>}) &= \sum_{i_1=1}^{m_1} \dots \sum_{i_p=1}^{m_p} \mathcal{X}(i_1, i_2, \dots, i_p) \text{vec} \left( \left( \bigotimes_{q=l}^1 e_{i_q}^{m_q} \right) \left( \bigotimes_{q=p}^{l+1} e_{i_q}^{m_q} \right)' \right) \\ &= \sum_{i_1=1}^{m_1} \dots \sum_{i_p=1}^{m_p} \mathcal{X}(i_1, i_2, \dots, i_p) \left( \bigotimes_{q=p}^1 e_{i_q}^{m_q} \right) = \text{vec}(\mathcal{X}). \end{aligned}$$

(c) Using the definition of vectorization in Table I, we have

$$\begin{aligned} (\text{vec } \mathcal{X})' (\text{vec } \mathcal{Y}) &= \left[ \sum_{i_1=1}^{m_1} \dots \sum_{i_p=1}^{m_p} \mathcal{X}(i_1, i_2, \dots, i_p) \left( \bigotimes_{q=p}^1 e_{i_q}^{m_q} \right)' \right] \left[ \sum_{i_1=1}^{m_1} \dots \sum_{i_p=1}^{m_p} \mathcal{Y}(i_1, i_2, \dots, i_p) \left( \bigotimes_{q=p}^1 e_{i_q}^{m_q} \right) \right] \\ &= \sum_{i_1=1}^{m_1} \dots \sum_{i_p=1}^{m_p} \mathcal{X}(i_1, i_2, \dots, i_p) \mathcal{Y}(i_1, i_2, \dots, i_p) \left( \bigotimes_{q=p}^1 e_{i_q}^{m_q} \right)' \left( \bigotimes_{q=p}^1 e_{i_q}^{m_q} \right) \\ &= \sum_{i_1=1}^{m_1} \dots \sum_{i_p=1}^{m_p} \mathcal{X}(i_1, i_2, \dots, i_p) \mathcal{Y}(i_1, i_2, \dots, i_p) = \langle \mathcal{X}, \mathcal{Y} \rangle. \end{aligned}$$

Similarly,

$$\begin{aligned} \text{tr}(\mathcal{X}_{(k)} \mathcal{Y}'_{(k)}) &= \text{tr} \left\{ \left[ \sum_{i_1=1}^{m_1} \dots \sum_{i_p=1}^{m_p} \mathcal{X}(i_1, i_2, \dots, i_p) (e_{i_k}^{m_k}) \left( \bigotimes_{\substack{q=p \\ q \neq k}}^1 e_{i_q}^{m_q} \right)' \right] \right. \\ &\quad \left. \left[ \sum_{i_1=1}^{m_1} \dots \sum_{i_p=1}^{m_p} \mathcal{Y}(i_1, i_2, \dots, i_p) \left( \bigotimes_{\substack{q=p \\ q \neq k}}^1 e_{i_q}^{m_q} \right) (e_{i_k}^{m_k})' \right] \right\} \\ &= \sum_{i_1=1}^{m_1} \dots \sum_{i_p=1}^{m_p} \mathcal{X}(i_1, i_2, \dots, i_p) \mathcal{Y}(i_1, i_2, \dots, i_p) \text{tr} \left\{ e_{i_k}^{m_k} \left( \bigotimes_{\substack{q=p \\ q \neq k}}^1 e_{i_q}^{m_q} \right)' \left( \bigotimes_{\substack{q=p \\ q \neq k}}^1 e_{i_q}^{m_q} \right) (e_{i_k}^{m_k})' \right\} \\ &= \sum_{i_1=1}^{m_1} \dots \sum_{i_p=1}^{m_p} \mathcal{X}(i_1, i_2, \dots, i_p) \mathcal{Y}(i_1, i_2, \dots, i_p) = \langle \mathcal{X}, \mathcal{Y} \rangle. \end{aligned}$$

(d) We have

$$\begin{aligned}\text{vec}[\mathcal{X}; A_1, \dots, A_p] &= \sum_{i_1=1}^{m_1} \dots \sum_{i_p=1}^{m_p} \mathcal{X}(i_1, i_2, \dots, i_p) \text{vec} \left( \bigcirc_{q=1}^p A_q(:, i_q) \right) \\ &= \sum_{i_1=1}^{m_1} \dots \sum_{i_p=1}^{m_p} \mathcal{X}(i_1, i_2, \dots, i_p) \left( \bigotimes_{q=p}^1 A_q(:, i_q) \right) = \left( \bigotimes_{q=p}^1 A_q \right) \text{vec}(\mathcal{X}).\end{aligned}$$

(e) We have

$$\begin{aligned}\mathcal{B}'_{\langle p \rangle} \text{vec } \mathcal{X} &= \left[ \sum_{i_1=1}^{m_1} \dots \sum_{i_p=1}^{m_p} \sum_{j_1=1}^{h_1} \dots \sum_{j_q=1}^{h_q} \mathcal{B}(i_1, \dots, i_p, j_1, \dots, j_q) \left( \left( \bigotimes_{k=q}^1 e_{j_k}^{h_k} \right) \left( \bigotimes_{k=p}^1 e_{i_k}^{m_k} \right)' \right) \right] \\ &\quad \times \left[ \sum_{i_1=1}^{m_1} \dots \sum_{i_p=1}^{m_p} \mathcal{X}(i_1, \dots, i_p) \left( \bigotimes_{k=p}^1 e_{i_k}^{m_k} \right) \right] \\ &= \sum_{i_1=1}^{m_1} \dots \sum_{i_p=1}^{m_p} \sum_{j_1=1}^{h_1} \dots \sum_{j_q=1}^{h_q} \mathcal{B}(i_1, \dots, i_p, j_1, \dots, j_q) \mathcal{X}(i_1, \dots, i_p) \left( \bigotimes_{k=q}^1 e_{j_k}^{h_k} \right) \left( \bigotimes_{k=p}^1 e_{i_k}^{m_k} \right)' \left( \bigotimes_{k=p}^1 e_{i_k}^{m_k} \right) \\ &= \sum_{i_1=1}^{m_1} \dots \sum_{i_p=1}^{m_p} \sum_{j_1=1}^{h_1} \dots \sum_{j_q=1}^{h_q} \mathcal{B}(i_1, \dots, i_p, j_1, \dots, j_q) \mathcal{X}(i_1, \dots, i_p) \left( \bigotimes_{k=q}^1 e_{j_k}^{h_k} \right) = \text{vec} \langle \mathcal{X} | \mathcal{B} \rangle.\end{aligned}$$

(f) Because of Lemma II.1(1) and Lemma II.1(2) and the commutation matrix, if  $\mathcal{Y} \in \mathbb{R}^{m_1 \times m_2 \times \dots \times m_k}$ , then

$$\text{vec}(\mathcal{Y}) = \text{vec}(\mathcal{Y}_{\langle k-1 \rangle}) = \text{vec}(\mathcal{Y}'_{(k)}) = K_{m_k, \prod_{i=1}^{k-1} m_i} \text{vec}(\mathcal{Y}_{(k)}). \quad (\text{S7})$$

Therefore, if we let  $\mathcal{X}^{(j_{k+1}, \dots, j_p)} \in \mathbb{R}^{m_1 \times m_2 \times \dots \times m_k}$  be the sub-tensor of  $\mathcal{X}$  defined as  $\mathcal{X}^{(j_{k+1}, \dots, j_p)} = \mathcal{X}(:, \dots, :, j_{k+1}, \dots, j_p)$ , then from (S7),

$$\begin{aligned}\text{vec}(\mathcal{X}) &= \begin{bmatrix} \text{vec } \mathcal{X}^{(1, \dots, 1, 1)} \\ \text{vec } \mathcal{X}^{(1, \dots, 1, 2)} \\ \vdots \\ \text{vec } \mathcal{X}^{(m_{k+1}, \dots, m_p)} \end{bmatrix} = \begin{bmatrix} K_{m_k, \prod_{i=1}^{k-1} m_i} \text{vec}(\mathcal{X}_{(k)}^{(1, \dots, 1, 1)}) \\ K_{m_k, \prod_{i=1}^{k-1} m_i} \text{vec}(\mathcal{X}_{(k)}^{(1, \dots, 1, 2)}) \\ \vdots \\ K_{m_k, \prod_{i=1}^{k-1} m_i} \text{vec}(\mathcal{X}_{(k)}^{(m_{k+1}, \dots, m_p)}) \end{bmatrix} \\ &= K'_{(k)} \text{vec}(\mathcal{X}_{(k)}).\end{aligned}$$

The result follows by left-multiplying both sides by the orthogonal matrix  $K_{(k)}$ .  $\square$

#### D. Proof of Theorem II.1

*Proof.*

(a) We have

$$\begin{aligned}(\circ \llbracket M_1, M_2, \dots, M_p \rrbracket)_{\langle p \rangle} &= \sum_{i_1=1}^{m_1} \sum_{j_1=1}^{h_1} \dots \sum_{i_p=1}^{m_p} \sum_{j_p=1}^{h_p} \left( \prod_{q=1}^p M_q(i_q, j_q) \right) \left\{ \left( \bigcirc_{q=1}^p e_{j_q}^{h_q} \right) \circ \left( \bigcirc_{q=1}^p e_{i_q}^{m_q} \right) \right\}_{\langle p \rangle} \\ &= \sum_{i_1=1}^{m_1} \sum_{j_1=1}^{h_1} \dots \sum_{i_p=1}^{m_p} \sum_{j_p=1}^{h_p} \left( \prod_{q=1}^p M_q(i_q, j_q) \right) \left\{ \left( \bigotimes_{q=p}^1 e_{j_q}^{h_q} \right) \left( \bigotimes_{q=p}^1 e_{i_q}^{m_q} \right)' \right\} \\ &= \sum_{i_1=1}^{m_1} \sum_{j_1=1}^{h_1} \dots \sum_{i_p=1}^{m_p} \sum_{j_p=1}^{h_p} \left( \prod_{q=1}^p M_q(i_q, j_q) \right) \left\{ \bigotimes_{q=p}^1 (e_{j_q}^{h_q} e_{i_q}^{m_q'}) \right\} = \bigotimes_{q=p}^1 M'_q.\end{aligned}$$

(b) Because of part (a) and Lemma II.1(5),

$$\text{vec} \langle \mathcal{X} | \circ \llbracket M_1, M_2, \dots, M_p \rrbracket \rangle = (\circ \llbracket M_1, M_2, \dots, M_p \rrbracket)_{\langle p \rangle}' \text{vec}(\mathcal{X}) = \left( \bigotimes_{q=p}^1 M_q \right) \text{vec}(\mathcal{X}) = \text{vec}[\mathcal{X}; M_1, \dots, M_p].$$

Therefore  $\llbracket \mathcal{X}; M_1, \dots, M_p \rrbracket$  and  $\langle \mathcal{X} | \circ \llbracket M_1, M_2, \dots, M_p \rrbracket \rangle$  are of the same size and vectorization, and must be the same.

(c)

$$\begin{aligned}
\circ[M_1, M_2, \dots, M_p]_{(\mathcal{R} \times \mathcal{C})} &= \sum_{i_1=1}^{m_1} \sum_{j_1=1}^{h_1} \dots \sum_{i_p=1}^{m_p} \sum_{j_p=1}^{h_p} \left( \prod_{q=1}^p M_q(i_q, j_q) \right) \left\{ \left( \overset{p}{\underset{q=1}{\circ}} e_{j_q}^{h_q} \right) \circ \left( \overset{p}{\underset{q=1}{\circ}} e_{i_q}^{m_q} \right) \right\}_{(\mathcal{R} \times \mathcal{C})} \\
&= \sum_{i_1=1}^{m_1} \sum_{j_1=1}^{h_1} \dots \sum_{i_p=1}^{m_p} \sum_{j_p=1}^{h_p} \left( \prod_{q=1}^p M_q(i_q, j_q) \right) \left\{ (e_{j_k}^{h_k} \otimes e_{i_k}^{m_k}) \left( \bigotimes_{q=p, q \neq k}^1 e_{j_q}^{h_q} \otimes \bigotimes_{q=p, q \neq k}^1 e_{i_q}^{m_q} \right)' \right\} \\
&= (\text{vec } M'_k) (\text{vec } \circ[M_1, M_2, \dots, M_{k-1}, M_{k+1}, \dots, M_p])'.
\end{aligned}$$

□

## S2. SUPPLEMENT TO SECTION III

### A. Some matrices involved in our methodology

In this Section we provide and simplify some expressions involved in Sections III-B and III-C. If  $\mathcal{V}$  is a tensor of size  $r \times r \times \dots \times r$ , then its super-diagonal  $\mathbf{v} \in \mathbb{R}^d$  contains the elements with coincident indices in each dimension of  $\mathcal{V}$ , such that

$$\mathbf{v}(i) = \mathcal{V}(i, i, \dots, i). \quad (\text{S8})$$

1) *The CP format:* Here we simplify some of the expressions involved in the CP format using the Hadamard (or element-wise) matrix-product  $(*)$ , which is computationally cheaper than the traditional matrix product. First, let  $\mathbf{w}_i$  be the super-diagonal of  $[\mathcal{X}_i; L'_1, L'_2, \dots, L'_l]$ , as defined in equation (S8). Then the matrix  $G_{ik}^{CP}$  in (38) can be simplified as

$$G_{ik}^{CP} = \begin{bmatrix} \mathbf{w}_i(1) & & \\ & \ddots & \\ & & \mathbf{w}_i(r) \end{bmatrix} \left( \bigodot_{q=p, q \neq k}^1 M_q \right)',$$

where  $\odot$  is the Khatri-Rao matrix product. This formulation allows us to simplify the matrix  $\sum_{i=1}^n G_{ik}^{CP} \Sigma_k^{-1} G_{ik}^{CP'}$  from Equation (40) using Proposition 3.2 from [26] as

$$\sum_{i=1}^n G_{ik}^{CP} \Sigma_k^{-1} G_{ik}^{CP'} = \left[ \sum_{i=1}^n \mathbf{w}_i \mathbf{w}_i' \right] * \left[ \overset{p}{*}_{q=1, q \neq k} (M'_k \Sigma_k^{-1} M_k) \right].$$

Similarly, the matrix  $\sum_{i=1}^n H_{ik}^{CP} \Sigma^{-1} H_{ik}^{CP'}$  from equation (42) can be written as  $\mathcal{H}_{<2>}^2$ , which is the 2-canonical matricization of the tensor  $\mathcal{H}^2$  of size  $l_k \times r \times l_k \times r$ , with sub-tensors

$$\mathcal{H}^2(s, :, t, :) = \left( \overset{p}{*}_{k=1} M'_k \Sigma_k^{-1} M_k \right) * \left( \sum_i^n \mathbf{w}_{si} \mathbf{w}_{ti}' \right) \quad \text{for all } s, t = 1, 2, \dots, r,$$

where  $\mathbf{w}_{si} \in \mathbb{R}^r$  is the super-diagonal of  $[\mathcal{X}_{si}; L'_1, \dots, L'_{k-1}, L'_{k+1}, \dots, L'_l]$ , and  $\mathcal{X}_{si}$  is the tensor of size  $h_1 \times \dots \times h_{k-1} \times h_{k+1} \times \dots \times h_l$  obtained upon fixing the  $k$ -th mode of  $\mathcal{X}_i$  at the position  $s$ .

2) *The TR format:* To define the matrices  $G_{ik}^{TR}$  for  $k = 1, 2, \dots, l$ , let

$$\mathcal{B}_{-\mathcal{M}_k} = \mathcal{M}_{k+1} \times^1 \dots \times^1 \mathcal{M}_p \times^1 \mathcal{L}_1 \times^1 \dots \times^1 \mathcal{L}_l \times^1 \mathcal{M}_1 \times^1 \dots \times^1 \mathcal{M}_{k-1}, \quad (\text{S9})$$

be the  $(p+1)$ th order TT-formatted tensor of dimension  $(g_k \times m_{k+1} \times \dots \times m_p \times h_1 \times \dots \times h_l \times m_1 \times \dots \times m_{k-1} \times g_{k-1})$  that is generated similar to the TR tensor in Equation (46), but is missing the TR factor  $\mathcal{M}_k$ . The tensor  $\mathcal{B}_{-\mathcal{M}_k}$  in Equation (S9) is defined for the cases where  $k = 2, 3, \dots, p-1$ , however  $\mathcal{B}_{-\mathcal{M}_1}$  and  $\mathcal{B}_{-\mathcal{M}_p}$  are similar: the tensor  $\mathcal{B}_{-\mathcal{M}_p}$  has dimensions  $(g_p \times h_1 \times \dots \times h_l \times m_1 \times \dots \times m_{p-1} \times g_{p-1})$  because  $\mathcal{L}_1$  is the first factor in the train, and the tensor  $\mathcal{B}_{-\mathcal{M}_1}$  has dimensions  $(g_1 \times m_2 \times \dots \times m_p \times h_1 \times \dots \times h_l \times g_0)$  because  $\mathcal{L}_l$  is the last factor in the train. We define the matrix  $G_{ik}^{TR}$  involved in Equation (47) as

$$G_{ik}^{TR} = \left\{ \mathcal{X}_i \times_{1,2,\dots,l}^{p-k+2, p-k+3, \dots, p-k+l+1} \mathcal{B}_{-\mathcal{M}_k} \right\}_{(\mathcal{R} \times \mathcal{C})},$$

where  $\mathcal{R} = \{1, p+1\}$ , and  $\mathcal{C}$  is the ordered set of size  $p-1$  that indexes the modes of size  $(m_1, m_2, \dots, m_p)$ , but skipping  $m_k$  and in reverse order (so that the order of the modes matches with the columns of  $\mathcal{Y}_{i(k)}$  in Equation (47)). Similarly, to define the matrices  $H_{ik}^{TR}$  for  $k = 1, 2, \dots, l$ , let

$$\mathcal{B}_{-\mathcal{L}_k} = \mathcal{L}_{k+1} \times^1 \dots \times^1 \mathcal{L}_l \times^1 \mathcal{M}_1 \times^1 \dots \times^1 \mathcal{M}_p \times^1 \mathcal{L}_1 \times^1 \dots \times^1 \mathcal{L}_{k-1}, \quad (\text{S10})$$

be the  $(p+1)$ -th order TT-formatted tensor of dimensions  $(s_k \times h_{k+1} \times \dots \times h_l \times m_1 \times \dots \times m_p \times h_1 \times \dots \times h_{k-1} \times s_{k-1})$  that is generated similar to the TR tensor in Equation (46), but is missing the TR factor  $\mathcal{L}_k$ . The tensor  $\mathcal{B}_{-\mathcal{L}_k}$  in (S10)



is defined for the cases where  $k = 2, 3, \dots, l-1$ , however  $\mathcal{B}_{-\mathcal{L}_1}$  and  $\mathcal{B}_{-\mathcal{L}_l}$  are similar: the tensor  $\mathcal{B}_{-\mathcal{L}_l}$  has dimensions  $(s_l \times m_1 \times \dots \times m_p \times h_1 \times \dots \times h_{l-1} \times s_{l-1})$  because  $\mathcal{M}_1$  is the first factor in the train, and the tensor  $\mathcal{B}_{-\mathcal{L}_1}$  has dimensions  $(s_1 \times h_2 \times \dots \times h_l \times m_1 \times \dots \times m_p \times s_0)$  because  $\mathcal{M}_p$  is the last factor in the train. We define the matrix  $H_{ik}^{TR}$  involved in Equation (48) as

$$H_{ik}^{TR} = \left\{ \mathcal{X}_i \times_{1, \dots, k-1, k+1, \dots, l}^{l+p+2-k, \dots, l+p, 2, \dots, l-k+1} \mathcal{B}_{-\mathcal{L}^{(k)}} \right\}_{(\mathcal{R} \times \mathcal{C})}, \quad (\text{S11})$$

where  $\mathcal{R} = \{2, 1, p+3\}$ , and  $\mathcal{C} = \{p+2, p+1, \dots, 3\}$  is the ordered set of size  $p-1$  that indexes the modes of size  $(m_1, m_2, \dots, m_p)$ . Note that we define the contraction in Equation (S11) as  $(\times_{2, \dots, l}^{2, \dots, l-k+1})$  when  $k=1$  and as  $(\times_{1, \dots, l-1}^{l+p+2-k, \dots, l+p})$  when  $k=l$ .

### B. Proof of Theorem III.1

*Proof.* Based on Lemma II.1(4) and Equation (31), we obtain

$$\text{vec}(\hat{\mathcal{V}}) = [M' \Sigma^{-1} \otimes W^{-'}] \text{vec}(Y'), \quad (\text{S12})$$

where

$$\text{vec}(Y') \sim \mathcal{N}_{n \times m}((M \otimes W') \text{vec}(\mathcal{V}), \sigma^2 \Sigma \otimes \mathbf{I}_n). \quad (\text{S13})$$

Furthermore, because  $W^- = X'(XX')^{-1}L(L'L)^{-1}$  and both  $W^{-'}W'$  and  $M'\Sigma^{-1}M$  are identity matrices, we obtain based on (S12) and (S13) that

$$\text{vec}(\hat{\mathcal{V}}) \sim \mathcal{N}_q(\text{vec}(\mathcal{V}), \sigma^2 I_m \otimes ((L'L)^{-1}L'(XX')^{-1}L(L'L)^{-1})), \quad (\text{S14})$$

where  $q$  is the product of the Tucker rank. Now, because  $\hat{M}_k$  and  $\hat{L}_k$  are MLEs and they are identifiable given the rest, as  $n \rightarrow \infty$   $\hat{M}_k \xrightarrow{P} M_k$  and  $\hat{L}_k \xrightarrow{P} L_k$ , and therefore

$$\left( \bigotimes_{k=p}^1 \hat{M}_k \right) \otimes \left( \bigotimes_{k=l}^1 \hat{L}_k \right) \xrightarrow{P} M \otimes L. \quad (\text{S15})$$

The rest of the proof follows by left-multiplying the  $\text{vec}(\hat{\mathcal{V}})$  of (S14) by the left hand side of (S15) and applying Slutsky's theorem.  $\square$

### C. Proof of Theorem III.2

*Proof.* From Equations (40) and (42), we obtain that  $\text{vec}(\hat{L}_k) = A_k \mathbf{y}$  and  $\text{vec}(\hat{M}_k) = B_k \mathbf{y}$ , and thus

$$\hat{\boldsymbol{\theta}}_{CP} = R_{CP} \mathbf{y}. \quad (\text{S16})$$

Further, from our normality and independence assumptions,

$$\mathbf{y} = \begin{bmatrix} \text{vec}(\mathcal{Y}_1) \\ \vdots \\ \text{vec}(\mathcal{Y}_n) \end{bmatrix} \sim \mathcal{N}_{m \times n} \left( \begin{bmatrix} \text{vec}(\langle \mathcal{X}_1 | \mathcal{B} \rangle) \\ \vdots \\ \text{vec}(\langle \mathcal{X}_n | \mathcal{B} \rangle) \end{bmatrix}, \mathbf{I}_n \otimes \Sigma \right), \quad (\text{S17})$$

and from (S16) and (S17),

$$\hat{\boldsymbol{\theta}}_{CP} \sim \mathcal{N}_{R \times (\sum_{i=1}^p m_i + \sum_{i=1}^l h_i)}(\boldsymbol{\theta}_{CP}, R_{CP}(\mathbf{I}_n \otimes \Sigma)R_{CP}').$$

Now consider the transformation  $g: \mathbb{R}^{R \times (\sum_{i=1}^p m_i + \sum_{i=1}^l h_i)} \rightarrow \mathbb{R}^{m \times h}$  such that  $g(\hat{\boldsymbol{\theta}}_{CP}) = \text{vec}(\hat{\mathcal{B}}_{CP})$ . The Jacobian matrix of this transformation is defined as

$$J_{CP} = \frac{\partial \text{vec}(\hat{\mathcal{B}}_{CP})}{\partial \hat{\boldsymbol{\theta}}_{CP}},$$

and is a block matrix with blocks as in Lemma S2.1(a). Using the multivariate extension of Taylor's theorem as in Theorem 5.2.3 in [75], we obtain

$$g(\hat{\boldsymbol{\theta}}_{CP}) \xrightarrow{d} \mathcal{N}_{m \times h} \left( g(\boldsymbol{\theta}_{CP}), J_{CP} R_{CP}(\mathbf{I}_n \otimes \Sigma) R_{CP}' J_{CP}' \right),$$

where  $g(\hat{\boldsymbol{\theta}}_{CP}) = \text{vec}(\hat{\mathcal{B}}_{CP})$  and  $g(\boldsymbol{\theta}_{CP}) = \text{vec}(\mathcal{B}_{CP})$ .  $\square$

#### D. Jacobian matrices

The Jacobians needed in Theorem III.1 are block matrices, where each block is given in the following lemma

##### Lemma S2.1.

(a) Let  $\mathcal{B}_{CP} = \llbracket M_1, M_2, \dots, M_p \rrbracket \in \mathbb{R}^{m_1 \times m_2 \times \dots \times m_p}$ . Then for  $k = 1, 2, \dots, p$ ,

$$\frac{\partial \text{vec}(\mathcal{B}_{CP})}{\partial \text{vec}(M_k)} = K'_{(k)}(T_k \otimes I_{m_k}), \text{ where } T_k = \bigodot_{q=p, q \neq k}^1 M_q.$$

(b) Let  $\mathcal{B}_{TR} = \text{tr}(\mathcal{M}_1 \times^1 \mathcal{M}_2 \times^1 \dots \times^1 \mathcal{M}_p) \in \mathbb{R}^{m_1 \times m_2 \times \dots \times m_p}$ . Then for  $k = 1, 2, \dots, p$ ,

$$\frac{\partial \text{vec}(\mathcal{B}_{TR})}{\partial \text{vec}(\mathcal{M}_{k(2)})} = K'_{(k)}(S'_k \otimes I_{m_k}),$$

where

$$S_k = \text{tr}(\mathcal{M}_{k+1} \times^1 \dots \times^1 \mathcal{M}_p \times^1 \mathcal{M}_1 \times^1 \dots \times^1 \mathcal{M}_{k-1})_{(\{1, p+1\} \times \{2, 3, \dots, p\})}.$$

(c) Let  $\mathcal{B}_{OP} = \circ \llbracket M_1, M_2, \dots, M_p \rrbracket \in \mathbb{R}^{m_1 \times \dots \times m_p \times n_1 \times \dots \times n_p}$ . Then for  $k = 1, 2, \dots, p$ ,

$$\frac{\partial \text{vec}(\mathcal{B}_{OP})}{\partial \text{vec}(M'_k)} = K'_{(p+k)} K'_{(k+1)} \left( (\text{vec} \circ \llbracket M_1, \dots, M_{k-1}, M_{k+1}, \dots, M_p \rrbracket) \otimes I_{m_k n_k} \right).$$

*Proof.*

(a) First, because  $\mathcal{B}_{CP(k)} = M_k T'_k$ , we have

$$\frac{\partial \text{vec}(\mathcal{B}_{CP(k)})}{\partial \text{vec}(M_k)} = T_k \otimes I_{m_k}.$$

The result follows from Lemma II.1(6).

(b) The derivation of this results follows a similar path as in part (a) because  $\mathcal{B}_{TR(k)} = M_{k(2)} S_k$ .

(c) Let  $\mathcal{R}$  and  $\mathcal{C}$  be as in Theorem II.1(3). Then the vectorization of (10) results in

$$\frac{\partial \text{vec}(\mathcal{B}_{OP(\mathcal{R} \times \mathcal{C})})}{\partial \text{vec}(M'_k)} = \left( (\text{vec} \circ \llbracket M_1, \dots, M_{k-1}, M_{k+1}, \dots, M_p \rrbracket) \otimes I_{m_k n_k} \right).$$

The result follows from  $\text{vec}(\mathcal{B}_{OP(\mathcal{R} \times \mathcal{C})}) = K_{(k+1)} K_{(p+k)} \text{vec}(\mathcal{B}_{OP})$ , where  $K_{(k)}$  is orthogonal as in Lemma II.1(6).  $\square$

#### E. The OP and TR cases

We now state and prove some results on inference for the OP and TR format:

##### Theorem S2.1.

1) Consider Equation (20) with  $\mathcal{B} = \mathcal{B}_{TR}$  as in (46) with its analogue  $\hat{\mathcal{B}}_{TR}$  and

$$\hat{\theta}_{TR} = [\text{vec}(\hat{\mathcal{L}}_1)' \text{vec}(\hat{\mathcal{L}}_2)' \dots \text{vec}(\hat{\mathcal{L}}_l)' \text{vec}(\hat{\mathcal{M}}_{1(2)})' \text{vec}(\hat{\mathcal{M}}_{2(2)})' \dots \text{vec}(\hat{\mathcal{M}}_{3(2)})']'.$$

Then as  $n \rightarrow \infty$ ,

$$\text{vec}(\hat{\mathcal{B}}_{TR}) \xrightarrow{d} \mathcal{N}_{m \times h} \left( \text{vec}(\mathcal{B}_{TR}), J_{TR} R_{TR} (I_n \otimes \Sigma) R'_{TR} J'_{TR} \right),$$

where  $J_{TR} = \frac{\partial \text{vec}(\hat{\mathcal{B}}_{TR})}{\partial \hat{\theta}_{TR}}$  is a block matrix with blocks given in Lemma S2.1(b) and  $R_{TR}$  is equal to  $R_{CP}$  in part (a) after replacing  $(G_{ik}^{CP}, H_{ik}^{CP})$  with  $(G_{ik}^{TR}, H_{ik}^{TR})$ .

2) Now let Equation (20) have  $\mathcal{B} = \mathcal{B}_{OP}$  as in (43) with its analogue  $\hat{\mathcal{B}}_{OP}$  and

$$\hat{\theta}_{OP} = [\text{vec}(\hat{M}_1)' \text{vec}(\hat{M}_2)' \dots \text{vec}(\hat{M}_p)']',$$

Then as  $n \rightarrow \infty$ ,

$$\text{vec}(\hat{\mathcal{B}}_{OP}) \xrightarrow{d} \mathcal{N}_{m \times h} \left( \text{vec}(\mathcal{B}_{OP}), J_{OP} R_{OP} (I_n \otimes \Sigma) R'_{OP} J'_{OP} \right),$$

where  $J_{OP} = \frac{\partial \text{vec}(\hat{\mathcal{B}}_{OP})}{\partial \hat{\theta}_{OP}}$  is a block matrix with blocks given in Lemma S2.1(c) and  $R_{OP} = [B'_1 B'_2 \dots B'_p]'$ , where  $B_p$  is given in part (a) after replacing  $G_{ik}^{CP}$  with  $G_{ik}^{OP}$ .

*Proof.*

The proof of both parts is similar to that of Theorem III.2 and thus omitted.  $\square$

### F. Proof of Theorem III.3

*Proof.* Based on Section III-B1, the estimation of  $\mathcal{B}$  when the intercept is present can be performed by centering the covariates and responses. Let  $C_n = I_n - \frac{1}{n} \mathbf{1}_n \mathbf{1}_n'$ . For the Tucker case in Theorem III.1, let  $Y_c = [(\text{vec } \mathcal{Y}_1^c)(\text{vec } \mathcal{Y}_2^c) \dots (\text{vec } \mathcal{Y}_n^c)]$ , where  $\mathcal{Y}_i^c = \mathcal{Y}_i - \bar{\mathcal{Y}}$ . Then  $\text{vec}(Y_c') = (I_m \otimes C_n) \text{vec}(Y')$ , and similar to Equation (S12),

$$\text{vec}(\hat{\mathcal{V}}) = [M' \Sigma^{-1} \otimes W^{+'}](I_m \otimes C_n) \text{vec}(Y') = [M' \Sigma^{-1} \otimes W^{+'}] \text{vec}(Y'),$$

where the last equality follows because  $X \mathbf{1}_n = \mathbf{0}$  when the covariates are centered, and therefore  $W^{+'} \mathbf{1}_n = \mathbf{0}$  also. The remaining results follow using the same steps as in the proof of theorem III.1, but with centered covariates. For the CP case as in Theorem III.2, if  $\mathbf{y}_c = [(\text{vec } \mathcal{Y}_1^c)'(\text{vec } \mathcal{Y}_2^c)' \dots (\text{vec } \mathcal{Y}_n^c)']'$  are the centered responses, then  $\mathbf{y}_c = (C_n \otimes I_m) \mathbf{y}$ , and similar to Equation (S16),

$$\hat{\boldsymbol{\theta}}_{CP} = R_{CP}(C_n \otimes I_m) \mathbf{y} = R_{CP} \mathbf{y},$$

where the last step follows because  $R_{CP}(\mathbf{1}_n \otimes I_m) = \mathbf{0}$ . The rest results by following the same steps as in the proof of Theorem III.2, but with centered covariates. The proof of the TR and OP cases are similar and thus ignored.  $\square$

### G. Proof of Theorem III.4

*Proof.*

- (a) This statement follows upon expressing the Equation (16) as the MVMLR regression model of Equation (17), and then applying Theorem 15.4 in [73].
- (b) Equation (16) with  $\sigma^2 = 1$  can be expressed as

$$\mathcal{Z}_i = \mathcal{Y}_i - \langle \mathcal{X}_i | \mathcal{B} \rangle \stackrel{iid}{\sim} N_{m_1, m_2, \dots, m_p}(0, \Sigma_1, \Sigma_2, \dots, \Sigma_p), \quad i = 1, 2, \dots, n. \quad (\text{S18})$$

We will start by finding the diagonal of the block Fisher information matrix. We know from Theorem II.2c that

$$\mathcal{Z}_{i(k)} \sim \mathcal{N}_{m_k, m_{-k}}(0, \Sigma_k, \Sigma_{-k}) \quad (\text{S19})$$

for  $k = 1, \dots, p$ . We find the second differential of the loglikelihood of  $\mathcal{Z}_{i(k)}$  in (S19) with respect to  $\Sigma_k$  only as

$$\begin{aligned} \ell(\Sigma_k) &= -\frac{m_{-k}}{2} \log |\Sigma_k| - \frac{1}{2} \text{tr}(\Sigma_k^{-1} \mathcal{Z}_{i(k)} \Sigma_{-k}^{-1} \mathcal{Z}_{i(k)}'), \\ \partial \ell(\Sigma_k) &= -\frac{m_{-k}}{2} \text{tr}(\Sigma_k^{-1} \partial \Sigma_k) + \frac{1}{2} \text{tr}(\Sigma_k^{-1} \partial \Sigma_k \Sigma_k^{-1} \mathcal{Z}_{i(k)} \Sigma_{-k}^{-1} \mathcal{Z}_{i(k)}'), \\ \partial^2 \ell(\Sigma_k) &= \frac{m_{-k}}{2} \text{tr}(\Sigma_k^{-1} \partial \Sigma_k \Sigma_k^{-1} \partial \Sigma_k) - \text{tr}(\Sigma_k^{-1} \partial \Sigma_k \Sigma_k^{-1} \partial \Sigma_k \Sigma_k^{-1} \mathcal{Z}_{i(k)} \Sigma_{-k}^{-1} \mathcal{Z}_{i(k)}'). \end{aligned} \quad (\text{S20})$$

Now, based on Equation (S19),  $\mathcal{Z}_{i(k)} \Sigma_{-k}^{-1} \mathcal{Z}_{i(k)}' \sim \mathcal{W}_{m_k}(m_{-k}, \Sigma_k)$ , where  $\mathcal{W}$  denotes the Wishart distribution on  $m_k \times m_k$ -dimension random matrices and  $m_{-k}$  degrees of freedom. Therefore  $\mathbb{E}(\mathcal{Z}_{i(k)} \Sigma_{-k}^{-1} \mathcal{Z}_{i(k)}') = m_{-k} \Sigma_k$ . Thus using the duplication matrix and expressing the matrix trace as a vector inner product in Lemma II.1(a and c)

$$\mathbb{E}(-\partial^2 \ell(\Sigma_k)) = \frac{m_{-k}}{2} \text{tr}(\Sigma_k^{-1} \partial \Sigma_k \Sigma_k^{-1} \partial \Sigma_k) = \partial(\text{vech } \Sigma_k)' \left( \frac{m_{-k}}{2} D'_{m_{-k}} (\Sigma_k \otimes \Sigma_k) D_{m_{-k}} \right) \partial(\text{vech } \Sigma_k).$$

Now we find the element in the (2,1)th position of the block-Fisher information matrix. Finding this element is enough to find the rest of the Fisher information matrix because the order of the scale matrices in the TVN distribution can be permuted in concordance with the modes of the random tensor. Let  $\Sigma_{-12} = \bigotimes_{i=p}^3 \Sigma_i$  and  $m_{-12} = \prod_{i=3}^p m_i$ . Then based on the distribution of  $\mathcal{Z}_{i(1)}$  in (S19) we can write the log likelihood as

$$\begin{aligned} \ell(\Sigma_1, \Sigma_2) &= -\frac{1}{2} \text{tr}[(\Sigma_{-12}^{-1} \otimes \Sigma_2^{-1}) \mathcal{Z}_{i(1)}' \Sigma_1^{-1} \mathcal{Z}_{i(1)}] \quad (\text{by Property S1.2c}) \\ &= -\frac{1}{2} \text{vec}(\Sigma_{-12}^{-1} \otimes \Sigma_2^{-1})' (\mathcal{Z}_{i(1)} \otimes \mathcal{Z}_{i(1)})' \text{vec}(\Sigma_1^{-1}) \quad (\text{by Lemma II.1a,c}) \\ &= -\frac{1}{2} \text{vec}(\Sigma_2^{-1})' R'_{\Sigma_{-12}^{-1}} (\mathcal{Z}_{i(1)} \otimes \mathcal{Z}_{i(1)})' \text{vec}(\Sigma_1^{-1}), \quad (\text{by Property S1.1c}) \end{aligned} \quad (\text{S21})$$

Furthermore, if  $X \sim N_{m_1, m_2}(0, \Sigma_1, \Sigma_2)$ ,  $J^{k,l}$  is a single-entry matrix (with 1 at the position  $(k, l)$  and 0 everywhere else) and  $\Sigma_1^{1/2}[k, i] = \sigma_{ki}^1$ ,  $\Sigma_2^{1/2}[j, l] = \sigma_{jl}^2$ , then for  $Z \sim N_{p, r}(0, I_p, I_r)$ ,

$$\begin{aligned}
\mathbb{E}(X \otimes X) &= (\Sigma_1^{1/2} \otimes \Sigma_1^{1/2}) \mathbb{E}(Z \otimes Z) (\Sigma_2^{1/2} \otimes \Sigma_2^{1/2}) = (\Sigma_1^{1/2} \otimes \Sigma_1^{1/2}) \{J^{k,l}\}_{k,l} (\Sigma_2^{1/2} \otimes \Sigma_2^{1/2}) \\
&= \left\{ \sum_{i=1}^p \sum_{j=1}^r \sigma_{ki}^1 \Sigma_1^{1/2} J^{i,j} \Sigma_2^{1/2} \sigma_{jl}^2 \right\}_{k,l} \\
&= \left\{ \sum_{i=1}^p \sum_{j=1}^r \sigma_{ki}^1 \Sigma_1^{1/2}[:, i] \Sigma_2^{1/2}[j, :] \sigma_{jl}^2 \right\}_{k,l} \\
&= \left\{ \left( \sum_{i=1}^p \sigma_{ki}^1 \Sigma_1^{1/2}[:, i] \right) \left( \sum_{j=1}^r \Sigma_2^{1/2}[j, :] \sigma_{jl}^2 \right) \right\}_{k,l} \\
&= \left\{ [\sigma_{k1}^1 I_p \dots \sigma_{kp}^1 I_p] \text{vec}(\Sigma_1^{1/2}) \text{vec}(\Sigma_2^{1/2})' \begin{bmatrix} \sigma_{1l}^2 I_r \\ \vdots \\ \sigma_{rl}^2 I_r \end{bmatrix} \right\}_{k,l} \\
&= (\Sigma_1^{1/2} \otimes I_p) \text{vec}(\Sigma_1^{1/2}) \text{vec}(\Sigma_2^{1/2})' (\Sigma_2^{1/2} \otimes I_r) = \text{vec}(\Sigma_1) \text{vec}(\Sigma_2)'.
\end{aligned} \tag{S22}$$

To differentiate the negative loglikelihood of (S21), we use that if  $\Sigma$  is non-singular then,  $\frac{\partial \text{vec} \Sigma^{-1}}{\partial \text{vec} \Sigma} = -(\Sigma^{-1} \otimes \Sigma^{-1})$ , which follows from vectorizing both sides of  $\partial \Sigma^{-1} = -\Sigma^{-1} \partial \Sigma \Sigma^{-1}$ . From application of this operation to both sides of (S21) and taking expectation of (S22) results in

$$\begin{aligned}
-\mathbb{E} \left( \frac{\partial^2 \ell(\Sigma_1, \Sigma_2)}{\partial (\text{vec} \Sigma_2) \partial (\text{vec} \Sigma_1)'} \right) &= \frac{1}{2} (\Sigma_2^{-1} \otimes \Sigma_2^{-1}) R'_{\Sigma_{-12}^{-1}} \left\{ \mathbb{E}(\mathcal{Z}_{i(1)} \otimes \mathcal{Z}_{i(1)}) \right\}' (\Sigma_1^{-1} \otimes \Sigma_1^{-1}) \\
&= \frac{1}{2} (\Sigma_2^{-1} \otimes \Sigma_2^{-1}) R'_{\Sigma_{-12}^{-1}} \left\{ (\text{vec} \Sigma_1) (\text{vec}(\Sigma_{-12} \otimes \Sigma_2))' \right\}' (\Sigma_1^{-1} \otimes \Sigma_1^{-1}) \\
&= \frac{1}{2} (\Sigma_2^{-1} \otimes \Sigma_2^{-1}) R'_{\Sigma_{-12}^{-1}} \text{vec}(\Sigma_{-12} \otimes \Sigma_2) (\text{vec} \Sigma_1^{-1})' \\
&= \frac{1}{2} (\Sigma_2^{-1} \otimes \Sigma_2^{-1}) R'_{\Sigma_{-12}^{-1}} R_{\Sigma_{-12}} (\text{vec} \Sigma_2) (\text{vec} \Sigma_1^{-1})' \quad (\text{Lemma S1.1c}) \\
&= \frac{m_{-12}}{2} (\Sigma_2^{-1} \otimes \Sigma_2^{-1}) (\text{vec} \Sigma_2) (\text{vec} \Sigma_1^{-1})' \quad (\text{see below}) \\
&= \frac{m_{-12}}{2} (\text{vec} \Sigma_2^{-1}) (\text{vec} \Sigma_1^{-1})'.
\end{aligned}$$

The rest follows by multiplying  $D'_{m_1}$  on the left and  $D_{m_2}$  on the right. The following term simplifies greatly using Property S1.1 of the commutation matrix and Property S1.2 of the Kronecker product:

$$\begin{aligned}
R'_{\Sigma_{-12}^{-1}} R_{\Sigma_{-12}} &= \left( [((\text{vec} \Sigma_{-12}^{-1})' \otimes I_{m_2}) (I_{m_{-12}} \otimes K_{m_{-12}, m_2})] \otimes I_{m_2} \right) \\
&\quad \left( [(I_{m_{-12}} \otimes K_{m_2, m_{-12}}) (\text{vec} \Sigma_{-12} \otimes I_{m_2})] \otimes I_{m_2} \right) \\
&= \left( ((\text{vec} \Sigma_{-12}^{-1})' \otimes I_{m_2}) (I_{m_{-12}} \otimes K_{m_{-12}, m_2}) (I_{m_{-12}} \otimes K_{m_2, m_{-12}}) (\text{vec} \Sigma_{-12} \otimes I_{m_2}) \right) \otimes I_{m_2} \\
&= \left( ((\text{vec} \Sigma_{-12}^{-1})' \otimes I_{m_2}) (I_{m_2 \times m_{-12}^2}) (\text{vec} \Sigma_{-12} \otimes I_{m_2}) \right) \otimes I_{m_2} \\
&= \text{tr}(\Sigma_{-12}^{-1} \Sigma_{-12}) \otimes I_{m_2^2} = m_{-12} I_{m_2^2}.
\end{aligned}$$

(c) Let  $\mathbb{I}_{\Sigma_{12}}$  denote the first four block matrices of the Fisher information,

$$\mathbb{I}_{\Sigma_{12}} = \frac{nm_{-12}}{2} \begin{bmatrix} m_2 D'_{m_1} (\Sigma_1^{-1} \otimes \Sigma_1^{-1}) D_{m_1} & D'_{m_1} (\text{vec}(\Sigma_1^{-1}) \text{vec}(\Sigma_2^{-1})') D_{m_2} \\ D'_{m_2} (\text{vec}(\Sigma_2^{-1}) \text{vec}(\Sigma_1^{-1})') D_{m_1} & m_1 D'_{m_2} (\Sigma_2^{-1} \otimes \Sigma_2^{-1}) D_{m_2} \end{bmatrix} = \begin{bmatrix} A & B \\ B' & C \end{bmatrix}.$$

Using the result of Section 3.8 of [73], where  $E^-$  denotes the Moore-Penrose inverse of  $E$ , we obtain:

$$A^{-1} = \frac{2}{nm_{-1}} D_{m_1}^- (\Sigma_1 \otimes \Sigma_1) D_{m_1}'^{-1}, \quad C^{-1} = \frac{2}{nm_{-2}} D_{m_2}^- (\Sigma_2 \otimes \Sigma_2) D_{m_2}'^{-1},$$

and

$$BC^{-1}B' = \frac{nm_{-1}}{2m_1} D_{m_1}' (\text{vec} \Sigma_1^{-1}) (\text{vec} \Sigma_1^{-1})' D_{m_1}.$$

Using these results we obtain

$$\begin{aligned}\text{tr}(A^{-1}BC^{-1}B') &= \frac{1}{m_1} \text{tr} \left( D_{m_1}^-(\Sigma_1 \otimes \Sigma_1) D_{m_1}^{+'} D_{m_1}' (\text{vec } \Sigma_1^{-1}) (\text{vec } \Sigma_1^{-1})' D_{m_1} \right) \\ &= \frac{1}{m_1} \text{tr} \left( D_{m_1}^-(\text{vec } \Sigma_1) (\text{vec } \Sigma_1^{-1})' D_{m_1} \right) = \frac{m_1}{m_1} = 1.\end{aligned}$$

This last result implies that for the Schur complement of  $\mathbb{I}_{\Sigma_{12}}$ , namely  $S = (A - BC^{-1}B')$ , it follows that  $S[A^{-1}D_{m_1}'(\text{vec } \Sigma_1^{-1})] = \mathbf{0}$ , which means that the  $S$  has a non-trivial kernel, and therefore is singular. So  $\mathbb{I}_{\Sigma_{12}}$  is singular [76], and consequently so is  $\mathbb{I}_{\Sigma}$ .  $\square$

## REFERENCES

- [1] R. A. Johnson and D. W. Wichern, *Applied multivariate statistical analysis*. Pearson, 2008.
- [2] R. Tibshirani, "Regression Shrinkage and Selection Via the Lasso," *Journal of the Royal Statistical Society: Series B (Methodological)*, vol. 58, no. 1, pp. 267–288, Jan. 1996.
- [3] J. Friedman, T. Hastie, and R. Tibshirani, "Sparse inverse covariance estimation with the graphical lasso," *Biostatistics*, vol. 9, no. 3, pp. 432–441, Jul. 2008.
- [4] R. D. Cook, B. Li, and F. Chiaromonte, "Envelope models for parsimonious and efficient multivariate liner regression," *Statistica Sinica*, vol. 20, no. 3, pp. 927–960, 2010.
- [5] A. Mukherjee and J. Zhu, "Reduced rank ridge regression and its kernel extensions," *Statistical Analysis and Data Mining*, vol. 4, no. 6, pp. 612–622, Dec. 2011.
- [6] M. E. Timmerman, "Multilevel component analysis," *British Journal of Mathematical and Statistical Psychology*, vol. 59, no. 2, pp. 301–320, 2006.
- [7] R. Bro, "Review on multiway analysis in chemistry—2000–2005," *Critical Reviews in Analytical Chemistry*, vol. 36, no. 3–4, pp. 279–293, 2006.
- [8] J. Liu, P. Musialski, P. Wonka, and J. Ye, "Tensor completion for estimating missing values in visual data," *IEEE Transactions on Pattern Analysis and Machine Intelligence*, vol. 35, no. 1, pp. 208–220, 2013.
- [9] A. Cichocki, D. Mandic, L. D. Lathauwer, G. Zhou, Q. Zhao, C. Caiafa, and H. A. Phan, "Tensor decompositions for signal processing applications: From two-way to multiway component analysis," *IEEE Signal Processing Magazine*, vol. 32, no. 2, 2015.
- [10] X. Li, H. Zhou, and L. Li, "Tucker tensor regression and neuroimaging analysis," *Statistics in Biosciences*, Mar 2018.
- [11] K. A. Busch, J. Fawcett, and D. G. Jacobs, "Clinical correlates of inpatient suicide," *Journal of clinical psychiatry*, vol. 64, 2003.
- [12] M. A. Just, L. Pan, V. L. Cherkassky, D. McMakin, C. Cha, M. K. Nock, and D. Brent, "Machine learning of neural representations of suicide and emotion concepts identifies suicidal youth," *Nature Human Behaviour*, vol. 1, pp. 911–919, 2017.
- [13] G. B. Huang, M. Ramesh, T. Berg, and E. Learned-Miller, "Labeled faces in the wild: A database for studying face recognition in unconstrained environments," University of Massachusetts, Amherst, Tech. Rep., October 2007.
- [14] M. Afifi and A. Abdelhamed, "Afif4: Deep gender classification based on adaboost-based fusion of isolated facial features and foggy faces," *Journal of Visual Communication and Image Representation*, vol. 62, pp. 77 – 86, 2019.
- [15] N. Kumar, A. C. Berg, P. N. Belhumeur, and S. K. Nayar, "Attribute and simile classifiers for face verification," in *2009 IEEE 12th International Conference on Computer Vision*, Sep. 2009, pp. 365–372.
- [16] J. D. Carroll and J.-J. Chang, "Analysis of individual differences in multidimensional scaling via an n-way generalization of "Eckart-Young" decomposition," *Psychometrika*, vol. 35, no. 3, pp. 283–319, Sep. 1970.
- [17] R. A. Harshman, "Foundations of the parafac procedure: Models and conditions for an explanatory" multi-modal factor analysis," *UCLA Working Papers in Phonetics*, no. 16, 1970.
- [18] L. R. Tucker, "Some mathematical notes on three-mode factor analysis," *Psychometrika*, vol. 31, no. 3, pp. 279–311, Sep 1966.
- [19] T. G. Kolda and B. W. Bader, "Tensor decompositions and applications," *SIAM Review*, vol. 51, no. 3, pp. 455–500, September 2009.
- [20] Q. Zhao, G. Zhou, S. Xie, L. Zhang, and A. Cichocki, "Tensor ring decomposition," *CoRR*, vol. abs/1606.05535, 2016.
- [21] I. Oseledets, "Tensor-train decomposition," *SIAM Journal on Scientific Computing*, vol. 33, no. 5, pp. 2295–2317, 2011.
- [22] P. Hoff, "Separable covariance arrays via the tucker product, with applications to multivariate relational data," *Bayesian Anal.*, vol. 6, no. 2, pp. 179–196, 06 2011.
- [23] D. Akdemir and A. Gupta, "Array variate random variables with multiway kronecker delta covariance matrix structure," *Journal of Algebraic Statistics*, vol. 2, pp. 98–113, 01 2011.
- [24] M. Ohlson, M. R. Ahmad, and D. von Rosen, "The multilinear normal distribution: Introduction and some basic properties," *Journal of Multivariate Analysis*, vol. 113, pp. 37 – 47, 2013.
- [25] A. M. Manceur and P. Dutilleul, "Maximum likelihood estimation for the tensor normal distribution: Algorithm, minimum sample size, and empirical bias and dispersion," *Journal of Computational and Applied Mathematics*, vol. 239, pp. 37 – 49, 2013.
- [26] T. G. Kolda, "Multilinear operators for higher-order decompositions," Sandia National Laboratories, Tech. Rep. SAND2006-2081, 923081, Apr. 2006.
- [27] A. Cichocki, N. Lee, I. Oseledets, A.-H. Phan, Q. Zhao, and D. P. Mandic, "Tensor networks for dimensionality reduction and large-scale optimization: Part 1 low-rank tensor decompositions," *Foundations and Trends® in Machine Learning*, vol. 9, no. 4–5, pp. 249–429, 2016.
- [28] L. De Lathauwer, B. De Moor, and J. Vandewalle, "A multilinear singular value decomposition," *SIAM Journal on Matrix Analysis and Applications*, vol. 21, no. 4, pp. 1253–1278, 2000.
- [29] D. Gerard and P. Hoff, "A higher-order LQ decomposition for separable covariance models," *Linear Algebra and its Applications*, vol. 505, pp. 57 – 84, 2016.
- [30] R. Orús, "A practical introduction to tensor networks: Matrix product states and projected entangled pair states," *Annals of Physics*, vol. 349, pp. 117 – 158, 2014.
- [31] G. Z. Thompson, R. Maitra, W. Q. Meeker, and A. Bastawros, "Classification with the matrix-variate- $\text{\$t}$  distribution," *arXiv:1907.09565 [stat]*, Jul. 2019, arXiv: 1907.09565.
- [32] A. Gupta and D. Nagar, *Matrix Variate Distributions*, ser. Monographs and Surveys in Pure and Applied Mathematics. Taylor & Francis, 1999.
- [33] M. M. Wolf, F. Verstraete, M. B. Hastings, and J. I. Cirac, "Area laws in quantum systems: Mutual information and correlations," *Physical review letters*, vol. 100, p. 070502, 03 2008.
- [34] M. S. Srivastava, T. von Rosen, and D. von Rosen, "Models with a kronecker product covariance structure: Estimation and testing," *Mathematical Methods of Statistics*, vol. 17, no. 4, pp. 357–370, Dec 2008.
- [35] J. de Leeuw, "Block-relaxation algorithms in statistics," in *Information Systems and Data Analysis*. Berlin, Heidelberg: Springer Berlin Heidelberg, 1994, pp. 308–324.
- [36] H. Abdi, "Singular value decomposition (svd) and generalized singular value decomposition (gsvd)," *Encyclopedia of Measurement and Statistics.*, 01 2007.

- [37] H. Glanz and L. Carvalho, "An expectation–maximization algorithm for the matrix normal distribution with an application in remote sensing," *Journal of Multivariate Analysis*, vol. 167, pp. 31 – 48, 2018.
- [38] E. Lock, "Tensor-on-tensor regression," *Journal of Computational and Graphical Statistics*, 01 2017.
- [39] P. Hoff, "Multilinear tensor regression for longitudinal relational data," *The Annals of Applied Statistics*, vol. 9, 11 2014.
- [40] C. Viroli, "On matrix-variate regression analysis," *Journal of Multivariate Analysis*, vol. 111, pp. 296 – 309, 2012.
- [41] S. Ding and R. Cook, "Matrix-variate regressions and envelope models," *Journal of the Royal Statistical Society: Series B (Statistical Methodology)*, vol. 80, 05 2016.
- [42] I. D. Currie, M. Durban, and P. H. C. Eilers, "Generalized Linear Array Models with Applications to Multidimensional Smoothing," *Journal of the Royal Statistical Society. Series B (Statistical Methodology)*, vol. 68, no. 2, pp. 259–280, 2006.
- [43] R. Kashyap, "A bayesian comparison of different classes of dynamic models using empirical data," *IEEE Transactions on Automatic Control*, vol. 22, no. 5, pp. 715–727, 1977.
- [44] G. Schwarz, "Estimating the dimension of a model," *Ann. Statist.*, vol. 6, no. 2, pp. 461–464, 03 1978. [Online]. Available: <http://dx.doi.org/10.1214/aos/1176344136>
- [45] K. V. Mardia, J. T. Kent, and J. M. Bibby, *Multivariate analysis*. New York: Academic Press, 1979.
- [46] R. Heller, D. Stanley, D. Yekutieli, N. Rubin, and Y. Benjamini, "Cluster-based analysis of fMRI data," *NeuroImage*, vol. 33, no. 2, pp. 599–608, nov 2006.
- [47] R. W. Cox, "AFNI: software for analysis and visualization of functional magnetic resonance neuroimages," *Computers and Biomedical research*, vol. 29, no. 3, pp. 162–173, 1996.
- [48] R. W. Cox and J. S. Hyde, "Software tools for analysis and visualization of fMRI data," *NMR in Biomedicine*, vol. 10, no. 4-5, pp. 171–178, 1997.
- [49] C. R. Genovese, N. A. Lazar, and T. Nichols, "Thresholding of statistical maps in functional neuroimaging using the false discovery rate," *Neuroimage*, vol. 15, pp. 870–878, 2002.
- [50] Y. Benjamini and R. Heller, "False discovery rates for spatial signals," *Journal of the American Statistical Association*, vol. 102, no. 480, pp. 1272–1281, 2007.
- [51] M. Smith and L. Fahrmeir, "Spatial Bayesian variable selection with application to functional Magnetic Resonance Imaging," *Journal of the American Statistical Association*, vol. 102, no. 478, pp. 417–431, 2007.
- [52] S. M. Smith and T. E. Nichols, "Threshold-free cluster enhancement: Addressing problems of smoothing, threshold dependence and localisation in cluster inference," *Neuroimage*, vol. 44, pp. 83–98, 2009.
- [53] K. Tabelow, J. Polzehl, H. U. Voss, and V. Spokoiny, "Analyzing fMRIexperiments with structural adaptive smoothing procedures," *NeuroImage*, vol. 33, no. 1, pp. 55–62, 2006.
- [54] J. Polzehl, H. U. Voss, and K. Tabelow, "Structural adaptive segmentation for statistical parametric mapping," *NeuroImage*, vol. 52, no. 2, pp. 515–523, 2010.
- [55] I. A. Almodóvar-Rivera and R. Maitra, "FAST adaptive smoothed thresholding for improved activation detection in low-signal fMRI," *IEEE Transactions on Medical Imaging*, vol. 38, no. 12, pp. 2821–2828, 2019.
- [56] W. Cheng, E. T. Rolls, J. Qiu, D. Yang, H. Ruan, D. Wei, L. Zhao, J. Meng, P. Xie, and J. Feng, "Functional Connectivity of the Precuneus in Unmedicated Patients With Depression," *Biological Psychiatry: Cognitive Neuroscience and Neuroimaging*, vol. 3, no. 12, pp. 1040–1049, Dec. 2018.
- [57] Y. Jacob, L. S. Morris, K.-H. Huang, M. Schneider, S. Rutter, G. Verma, J. W. Murrough, and P. Balchandani, "Neural correlates of rumination in major depressive disorder: A brain network analysis," *NeuroImage: Clinical*, vol. 25, p. 102142, Jan. 2020.
- [58] H.-X. Zhou, X. Chen, Y.-Q. Shen, L. Li, N.-X. Chen, Z.-C. Zhu, F. X. Castellanos, and C.-G. Yan, "Rumination and the default mode network: Meta-analysis of brain imaging studies and implications for depression," *NeuroImage*, vol. 206, p. 116287, Feb. 2020.
- [59] A. Bechara, H. Damasio, and A. R. Damasio, "Emotion, Decision Making and the Orbitofrontal Cortex," *Cerebral Cortex*, vol. 10, no. 3, pp. 295–307, Mar. 2000.
- [60] F. Jollant, N. S. Lawrence, V. Giampietro, M. J. Brammer, M. A. Fullana, D. Drapier, P. Courtet, and M. L. Phillips, "Orbitofrontal cortex response to angry faces in men with histories of suicide attempts," *The American Journal of Psychiatry*, vol. 165, no. 6, pp. 740–748, Jun. 2008.
- [61] A. B. Satpute and K. A. Lindquist, "The Default Mode Network's Role in Discrete Emotion," *Trends in Cognitive Sciences*, vol. 23, no. 10, pp. 851–864, Oct. 2019.
- [62] S. R. Simon, M. Meunier, L. Piettre, A. M. Berardi, C. M. Segebarth, and D. Boussaoud, "Spatial attention and memory versus motor preparation: premotor cortex involvement as revealed by fMRI," *Journal of Neurophysiology*, vol. 88, no. 4, pp. 2047–2057, Oct. 2002.
- [63] M. Koenigs, A. K. Barbey, B. R. Postle, and J. Grafman, "Superior Parietal Cortex Is Critical for the Manipulation of Information in Working Memory," *Journal of Neuroscience*, vol. 29, no. 47, pp. 14 980–14 986, Nov. 2009.
- [64] J. J. Maller, R. H. S. Thomson, J. V. Rosenfeld, R. Anderson, Z. J. Daskalakis, and P. B. Fitzgerald, "Occipital bending in depression," *Brain*, vol. 137, no. 6, pp. 1830–1837, Jun. 2014.
- [65] R. Smith, R. D. Lane, A. Alkozei, J. Bao, C. Smith, A. Sanova, M. Nettles, and W. D. S. Killgore, "The role of medial prefrontal cortex in the working memory maintenance of one's own emotional responses," *Scientific Reports*, vol. 8, no. 1, p. 3460, Feb. 2018.
- [66] E. T. Rolls, "The cingulate cortex and limbic systems for action, emotion, and memory," *Handbook of Clinical Neurology*, vol. 166, pp. 23–37, 2019.
- [67] E. J. Bubb, L. Kinnavane, and J. P. Aggleton, "Hippocampal – diencephalic – cingulate networks for memory and emotion: An anatomical guide," *Brain and Neuroscience Advances*, vol. 1, Aug. 2017.
- [68] S. R. Heilbronner, B. Y. Hayden, and M. L. Platt, "Decision Salience Signals in Posterior Cingulate Cortex," *Frontiers in Neuroscience*, vol. 5, Apr. 2011.
- [69] W. Zhao, K. M. Kendrick, F. Chen, H. Li, and T. Feng, "Neural circuitry involved in quitting after repeated failures: role of the cingulate and temporal parietal junction," *Scientific Reports*, vol. 6, no. 1, p. 24713, Apr. 2016.
- [70] D. Zaitchik, C. Walker, S. Miller, P. LaViolette, E. Feczko, and B. C. Dickerson, "Mental state attribution and the temporoparietal junction: An fMRI study comparing belief, emotion, and perception," *Neuropsychologia*, vol. 48, no. 9, pp. 2528–2536, Jul. 2010.
- [71] G. Lettieri, G. Handjaras, E. Ricciardi, A. Leo, P. Papale, M. Betta, P. Pietrini, and L. Cecchetti, "Emotionotopy in the human right temporo-parietal cortex," *Nature Communications*, vol. 10, no. 1, p. 5568, Dec. 2019.
- [72] L. G. Ungerleider, S. M. Courtney, and J. V. Haxby, "A neural system for human visual working memory," *Proceedings of the National Academy of Sciences*, vol. 95, no. 3, pp. 883–890, Feb. 1998.
- [73] J. R. Magnus and H. Neudecker, *Matrix differential calculus with applications in statistics and econometrics*, third edition ed., ser. Wiley series in probability and statistics. Wiley, 2019.
- [74] K. B. Petersen and M. S. Pedersen, "The matrix cookbook," nov 2012, version 20121115.
- [75] E. L. Lehmann, *Elements of large-sample theory*, ser. Springer texts in statistics. New York: Springer, 1999.
- [76] T.-T. Lu and S.-H. Shiou, "Inverses of 2 x 2 block matrices," *Computers & Mathematics with Applications*, vol. 43, no. 1, pp. 119–129, 2002.